KUOPION YLIOPISTON JULKAISUJA C. LUONNONTIETEET JA YMPÄRISTÖTIETEET 159
KUOPIO UNIVERSITY PUBLICATIONS C. NATURAL AND ENVIRONMENTAL SCIENCES 159

MIKKO LAASANEN

Development and Validation of Mechano-Acoustic Techniques and Instrument for Evaluation of Articular Cartilage

Doctoral dissertation

To be presented by permission of the Faculty of Natural and Environmental Sciences of the University of Kuopio for public examination in Auditorium L21, Snellmania building, University of Kuopio, Friday 31st October 2003, at 12 noon

Department of Applied Physics, University of Kuopio
Department of Anatomy, University of Kuopio
Department of Clinical Physiology and Nuclear Medicine,
Kuopio University Hospital and University of Kuopio

KUOPION YLIOPISTO
KUOPIO 2003

Distributor:

Kuopio University Library
P.O. Box 1627
FIN-70211 KUOPIO
FINLAND
Tel. +358 17 163 430
Fax +358 17 163 410
http://www.uku.fi/kirjasto/julkaisutoiminta/julkmyyn.html

Series Editors:

Professor Lauri Kärenlampi, Ph.D.
Department of Ecology and Environmental Science

Professor Jari Kaipio, Ph.D.
Department of Applied Physics

Author's address:

Department of Applied Physics
University of Kuopio
P.O. Box 1627
FIN-70211 KUOPIO
FINLAND
Tel. +358 17 163 014
Fax +358 17 163 032
E-mail: mikko.laasanen@uku.fi

Supervisors:

Docent Jukka Jurvelin, Ph.D.
Department of Applied Physics
University of Kuopio

Juha Töyräs, Ph.D.
Department of Applied Physics
University of Kuopio

Reviewers:

Professor Arthur F.T. Mak, Ph.D.
Jockey Club Rehabilitation Engineering Center
The Hong Kong Polytechnic University
Kowloon
Hong Kong

Associate Professor Jun-Kyo Francis Suh, Ph.D.
Department of Biomedical Engineering
Tulane University
New Orleans, LA
USA

Opponent:

Research Director Thomas M. Quinn, Ph.D.
Orthopaedic Research Laboratory
Federal Polytechnic Lausanne
Lausanne
Switzerland

ISBN 951-781-257-4
ISSN 1235-0486

Kopijyvä
Kuopio 2003
Finland

Laasanen, Mikko. Development and Validation of Mechano-Acoustic Techniques and Instrument for Evaluation of Articular Cartilage. Kuopio University Publications C. Natural and Environmental Sciences 159. 2003. 88 p.
ISBN 951-781-257-4
ISSN 1235-0486

ABSTRACT

Degenerative joint diseases, such as osteoarthrosis (OA), induce pain and loss of mobility to millions of people worldwide. During the early stages of OA, damage of the superficial collagen network of articular cartilage, depletion of proteoglycans and a reduction in cartilage stiffness take place. Current clinical methods for the diagnosis of OA include X-ray, magnetic resonance imaging and arthroscopy. These methods are only qualitative and may be insensitive at detecting the earliest signs of OA or monitoring the outcome of surgical cartilage repair in a quantitative manner.

In this study, an ultrasound indentation instrument, combining ultrasonic and mechanical measurements, was developed and validated experimentally and numerically for use in the quantitative evaluation of cartilage quality. *In vitro* and *in situ* tests were conducted with normal and enzymatically degraded bovine cartilage. In the ultrasound indentation, tissue thickness was calculated using a predefined sound speed. The measurement error induced by the use of the predefined, constant sound speed was investigated in normal, enzymatically degraded and spontaneously degenerated cartilage. In addition, ultrasound imaging and mechanical techniques were used for the evaluation of normal, degenerated and surgically repaired cartilage.

The novel instrument enabled quantitative measurements of the tissue thickness, stiffness (dynamic modulus), creep rate and ultrasound reflection from the cartilage surface. The use of a constant sound speed induced an error of <8% on the thickness and dynamic modulus. In the bovine knee, site-dependent variations in the cartilage mechanical and acoustic properties were revealed with a reference material testing device, as well as with the novel instrument. Further, enzymatic degradation of cartilage composition was sensitively and specifically detected with the ultrasound indentation instrument. Ultrasound reflection from the cartilage surface was the best method for detecting the collagen network damage, whereas cartilage equilibrium and time-dependent mechanical properties were related to proteoglycan depletion. Visual evaluation was a poor indicator of cartilage quality. Instead, ultrasound imaging and mechanical parameters, especially dynamic modulus, were sensitive at revealing cartilage degeneration. After the surgical autologous chondrocyte transplantation operation, ultrasound imaging provided detailed information on the structural integrity of the porcine cartilage and underlying bone.

To conclude, mechano-acoustic methods may significantly improve the diagnostics of OA, as well as monitoring the success of cartilage repair procedures. With the ultrasound indentation instrument, cartilage thickness, mechanical properties and status of the superficial collagen network can be determined quantitatively and reproducibly. In the future, the instrument may be used during arthroscopic examinations, helping to initiate preventive actions prior to permanent cartilage degeneration. Ultrasound imaging is suitable for detecting cartilage superficial degeneration and monitoring tissue integrity after surgical procedures. However, further technical development is still needed before these techniques can be used in routine clinical diagnostics.

National Library of Medicine Classification: QT 36, WE 26, WE 300, WE 348, WN 208
Medical Subject Headings: biomechanics; cartilage, articular / physiology; osteoarthritis / diagnosis; ultrasonics; ultrasonography; materials testing; collagen; proteoglycans; models, theoretical

To Jaana

ACKNOWLEDGMENTS

This study was carried out during the years 2000-2003 in the Departments of Anatomy and Applied Physics, University of Kuopio and in the Department of Clinical Physiology and Nuclear Medicine, Kuopio University Hospital. I am very grateful to Professor Heikki Helminen, M.D., Ph.D., for placing the resources of the Department of Anatomy at my disposal. He has been as a "research grandfather" of our research group and it has been a great honor that we have always been able to count on his knowledge and wise support.

I owe my deepest gratitude to my head supervisor, Docent Jukka Jurvelin, Ph.D., for his professional guidance and for the wisdom that he has shared. His truly constructive criticism, as well as optimism and encouragment, serve as a model to any researcher director.

I express my sincere thanks to my other supervisor, Juha Töyräs, Ph.D., for his extensive collaboration and for the practical supervision. It has been a great advantage to work with a senior researcher who shares endless expertise and has given support during every point of the research projects.

I am grateful to official pre-examiners Professor Arthur F.T. Mak, Ph.D., and Associate Professor Jun-Kyo Francis Suh, Ph.D., for their constructive criticism to improve this thesis. I give my cordial thanks also to Ewen MacDonald, D.Pharm, for revising the language of the thesis.

I cherish all members of the Biophysics of Bone and Cartilage group for their friendly and helpful attitude. Especially, Simo Saarakkala, B.Sc., is acknowledged for his continuous and ever enjoyable co-operation since the very beginning of our research studies. I am deeply indebted to Jani Hirvonen, B.Eng., M.Sc., for his software programming studies. Rami Korhonen, M.Sc., is warmly acknowledged for introducing me to the research of cartilage biomechanics and for fulfilling the finite-element analysis. Furthermore, I want to express my thanks to Jarno Rieppo, B.M., for the quantitative microscopical analysis and for his every day criticism. Physics student Jatta Kurkijärvi is acknowledged for her help with the biomechanical measurements. Professor Reijo Lappalainen, Ph.D. (Department of Applied Physics), as well as physics students Heikki Nieminen and Mikko Hakulinen are acknowledged for their bracing criticism and support during these years. I owe my thanks also to Miika Nieminen, Ph.D., (Oulu University Hospital) and physics student Mikko Nissi for their collaboration and introducing me to the LaTeX.

I express my gratitude to all of the personnel of the Department of Anatomy. Especially, Mrs. Eija Rahunen, Mrs. Elma Sorsa and Mr. Kari Kotikumpu are acknowledged for their help with the histological analysis and advice to the good laboratory practise. I wish to thank Mikko Lammi, Ph.D., and Kari Törrönen, M.Sc., for their help with the biochemical analysis. My thanks belong also to secretaries Mrs. Irma Pääkkönen, Mrs. Arja Hoffren and Mrs. Kati Bolodin for the

help with bureaucracy and to Mika Hyttinen, M.D., and Outi Pulliainen, M.Sc., for their help during the porcine project. Alpo Pelttari, M.Sc., is warmly appreciated for his technical assistance and for understanding that we had to borrow special implements from his inexhaustible toolbox.

My gratitude is addressed also to Ilkka Kiviranta, M.D., Ph.D., Jyväskylä Central Hospital, and Anna Vasara, M.D., Helsinki University Hospital, for the kind possibility to use surgically repaired porcine knees as a research material.

I want to thank Atria Lihakunta Oyj, Kuopio, and their personnel for the continuous possibility to use bovine and porcine knee joints as our research material. Artscan Oyj, Helsinki, Finland and the personnel of the technical department, University of Kuopio, are acknowledged for their technical support.

I send my dearest thanks to my parents, Salli and Heino Laasanen for their endless encouragement and much support during my all studies.

Finally, I want to express my deepest and dearest thanks to my beloved wife, Jaana, for her love and joy of living that she endows. Our shared "little adventures" have made my efforts possible and delightful.

This thesis work was financially supported by the following finnish institutions: the National Technology Agency (TEKES projects 40094/99 and 40714/01), Kuopio University Hospital (EVO grants 5103 and 5173), Finnish Graduate School in Skeletal Diseases and Biomaterial Research School. Finnish Cultural Foundation of Northern Savo, Research Foundation of Orion Pharma, Paulo Research Foundation, Kuopio University Foundation and High Technology Foundation of Eastern Finland are also acknowledged for their highly valuable personal grants.

Kuopio, October 2003

Mikko Laasanen

ABBREVIATIONS AND NOMENCLATURE

ACT	autologous chondrocyte transplantation
AIB	apparent integrated backscatter
CV	coefficient of variation
DD	digital densitometry
ePLM	enhanced polarized light microscopy
FE	finite-element
FMC	medial condyle of femur
FTIRI	Fourier transform infrared imaging
GAG	glycosaminoglycan
IRC	integrated reflection coefficient
LPG	lateral facet of the patello-femoral groove
MTP	medial tibial plateau
MPG	medial facet of the patello-femoral groove
MRI	magnetic resonance imaging
OA	osteoarthrosis
OCT	optical coherence tomography
OD	optical density
PAT	patella
PBS	phosphate buffered saline
PG	proteoglycan
PLM	polarized light microscopy
sCV	standardized coefficient of variation
SEM	standardized error of mean
SD	standard deviation
TOF	time of flight
A	amplitude of the signal
a	radius of the indenter (or ultrasound transducer)
a/h	area-aspect-ratio
$\mathcal{A}$	absorbance
B_s	elastic bulk modulus
B_W	beam width
b	path length of the light
C	concentration
c	sound speed
E	(elastic) Young's modulus
E_{dyn}	dynamic modulus
E_H	Hilbert's envelope

$\boldsymbol{e}^s$	deviatoric component of the solid strain tensor
F	focal length
F_D	depth of focal zone
f	frequency
H_a	aggregate modulus
h	thickness
h_H	fast Hilbert transform
I	intensity of the signal
$\mathbf{I}$	unity tensor
J	compliance
k	creep rate
k_p	permeability
n	number of samples
p	statistical significance
p_h	hydrostatic pressure
R	reflection coefficient
R_c	radius of curvature
r	Pearson correlation coefficient
$r_{Spearman}$	Spearman correlation coefficient
T	transmission coefficient
t	time
$\mathcal{T}$	transmittance
$\mathbf{v}$	velocity vector
$\bar{x}$	average
Z	acoustic impedance
ϵ and $\boldsymbol{\epsilon}$	strain and strain tensor
θ	angle
κ	theoretical correction coefficient (indentation geometry)
λ	wavelength
μ_s	elastic shear modulus
$\overline{\mu}$	average within population
ν	Poisson's ratio
$\boldsymbol{\pi}$	diffuse body force vector
ρ	material density
σ and $\boldsymbol{\sigma}$	stress and stress tensor
σ_x and σ_μ	SD and SD of the parameter within population
τ	retardation time
ϕ	volume fraction
ω_0	elastic displacement

LIST OF ORIGINAL PUBLICATIONS

This thesis is based on the following original articles, which are referred in the text by their Roman numerals (I-V):

I Laasanen MS, Töyräs J, Korhonen RK, Rieppo J, Saarakkala S, Nieminen MT, Hirvonen J, Jurvelin JS. Biomechanical properties of knee articular cartilage. *Biorheology* 40: 133-140, 2003.

II Laasanen MS, Töyräs J, Hirvonen J, Saarakkala S, Korhonen R, Nieminen MT, Kiviranta I, Jurvelin JS. Novel mechano-acoustic technique and instrument for diagnosis of cartilage degeneration.
Physiological Measurement 23: 491-503, 2002.

III Laasanen MS, Saarakkala S, Töyräs J, Hirvonen J, Rieppo J, Korhonen RK, Jurvelin JS. Ultrasound indentation of bovine articular cartilage *in situ*.
Journal of Biomechanics 36: 1259-1267, 2003.

IV Töyräs J, Laasanen MS, Saarakkala S, Lammi MJ, Rieppo J, Kurkijärvi J, Lappalainen R, Jurvelin JS. Speed of sound in normal and degenerated bovine articular cartilage.
Ultrasound in Medicine and Biology 29: 447-454, 2003.

V Laasanen MS, Töyräs J, Vasara AI, Hyttinen MM, Saarakkala S, Hirvonen J, Jurvelin JS, Kiviranta I. Mechano-acoustic diagnosis of cartilage degeneration and repair.
Journal of Bone & Joint Surgery (American), 85-A Suppl 2: 78-84, 2003.

The thesis contains also previously unpublished data.

CHAPTER I

Introduction

Articular cartilage is highly specialized tissue that protects the ends of articulating bones in the diarthrodial joints from the stresses associated with mechanical load bearing, friction and impact. Cartilage must be able to perform its essential physiological functions without suffering any damage over the lifespan of the human being. However, it has been estimated that, *e.g.*, in United States about 43 million individuals (1 out of 6) are affected by the different forms of osteoarthrosis (OA) (arthrosis, osteoarthritis, arthritis) which damages the composition, structure and functional properties of cartilage tissue. The prevalence and expensive medical care of OA, as well as working disabilities due to pain and loss of joint mobility, result in suffering and enormous annual financial expenses [48, 174].

The mechanical response of the articular cartilage to physiological loading is mostly governed by the interactions occurring between its main structural components, *i.e.* collagen (type II) fibrils, proteoglycan macromolecules (PGs) and water containing diffusible ions [117]. During the earliest stages of cartilage degeneration, such as in early OA, the PG content of the superficial tissue decreases, the water content increases and the organization of the collagen fibril network deteriorates. These structural changes are accompanied by the decrease of cartilage compressive stiffness [26, 116]. The injured cartilage tissue has only a limited capacity for self-repair and is vulnerable to further damage during subsequent joint loading. An injury to the collagen network is especially harmful to cartilage, since the resilience and tensile properties of the cartilage are widely maintained by the collagen network and in mature cartilage its disruption is known to be irreversible [26, 27, 118]. On the other hand, much of the reduction of cartilage PG content and compressive stiffness, related to short time immobilization, may be restored by appropriate physiological joint loading [63, 131]. Thus, a method capable of separating these degenerative processes could provide a new perspective for the diagnosis and treatment of early OA and rheumatic diseases.

In clinical practice, diagnosis of OA is based on the thinning and destruction

of the cartilage, as detected radiographically, using magnetic resonance imaging (MRI) or by visual evaluation and palpation during an arthroscopic examination. Unfortunately these techniques are insensitive in revealing the superficial PG or collagen degradation (radiographs show only joint space narrowing and subchondral bone sclerosis whereas the clinical MRI-techniques still suffer from inadequate resolution). The visual evaluation and manual palpation of the cartilage surface during arthroscopy are subjective methods for the evaluation of tissue stiffness. Instead, quantitative mechanical indentation measurements can be used for detecting articular cartilage softening during the initial phase of OA [8, 41, 102, 107]. In the clinical indentation measurements, however, the unknown tissue thickness limits the reliability of the indentation results, especially in the case of thin cartilage [69, 175].

Cartilagineus and osteochondral injuries are common after joint traumas. Local and confined cartilage-bone injuries may be treated with surgical cartilage repair methods [25, 31, 70]. Unfortunately, current clinical methods are not optimal for monitoring the success of surgical interventions. High resolution *in vivo* imaging techniques could provide a means for monitoring tissue maturation and for the delineation of the repair area before an operation. Furthermore, it would be desirable to use biomechanical measurements to follow the restoration of the tissue mechanical competence post-operatively [77].

Previous studies have shown that high frequency ultrasound measurements may be used for determining cartilage thickness [114, 143, 159] and the disruption of the superficial collagen network may be sensitively and selectively detected as a decrease of ultrasound reflection from the cartilage surface [124, 161]. In addition, ultrasound may provide information on cartilage structural integrity [2, 35, 46, 146] and, when combined with the mechanical indentation testing [85, 159, 177], quantitative mechanical parameters of the tissue may be determined in an objective manner.

The main aim of this thesis was to combine mechanical and acoustic measurements towards quantitative, arthroscopic evaluation of cartilage quality. A novel ultrasound indentation technique and instrument, combining ultrasonic and mechanical measurements, was designed, developed and experimentally and numerically validated. Experimental *in vitro* and *in situ* tests were conducted using bovine cartilage. Further, ultrasound imaging, combined with mechanical indentation, was used to evaluate the success of autologous chondrocyte transplantation surgery (ACT) in porcine articular cartilage.

CHAPTER II

Composition and structure of articular cartilage

2.1 Solid matrix and interstitial water

Articular cartilage is a fiber-reinforced composite material, containing two distinct phases. The solid phase, which is porous and permeable, is mainly made up of type II collagens, PGs and chondrocytes [67, 70, 116]. The fluid phase contains water and solutes, *i.e.* ions and nutrients. PGs and collagens play an important role in the mechanical response of the tissue. The solid matrix is anchored to the underlying subchondral bone and the fluid can flow in and out of the tissue. The unique load-carrying capability of articular cartilage arises from the highly evolved composition and structure of the tissue. The coefficient of friction between articulating surfaces is remarkably low during dynamic loading (in human joints 0.001 - 0.08 [51]). The low coefficient of friction results from the biphasic nature of cartilage [11, 51, 100] and the lubrication induced by the synovial fluid [51, 52]. Furthermore, it has been proposed that the joint specific glycoprotein, lubricin, is a critical component present in the layer of fluid between the opposing articular surfaces [27].

The material properties of cartilage depend on the extracellular matrix, whereas the existence and maintenance of the matrix rely on a relatively few active cells *i.e.* chondrocytes (<10% of the volume). Articular cartilage has neither blood vessels nor nerves and the cells receive nutrients through diffusion. In the skeletally mature cartilage, nutrients are obtained only from the synovival fluid, not from the subchondral bone [70].

PGs are made up of monomers, which are linked to a hyaluronic acid backbone by a link protein (Figure 2.1A). A PG monomer consists of numerous repeating units of glycosaminoglycans (chondroitin-4-sulfate and chondroitin-6-sulfate are the most common) linked to a protein core. The negatively charged glycosaminoglycan (GAG) side chains attract cations and water into the tissue, enhancing the tissue propensity to swell. PGs control the compressive properties especially at mechanical equilibrium [15, 16, 96, 116] and the transient viscoelastic creep and stress-relaxation

behaviors of the cartilage occur mainly through the interstitial fluid flow which is primarily controlled by the PGs.

Type II collagen forms fibrils which can withstand tension and thus they provide the high tensile stiffness and strength for the cartilage matrix [88, 116]. A tensile modulus of 270 MPa has been determined for a single human type II collagen molecule [160]. The tissue would swell considerably if the collagen fibrils were not able to effectively balance the swelling pressure of the PG-filled matrix [70, 116]. This interplay between the main constituents of the tissue and the intrinsic resistance of the solid matrix contributes to cartilage compressive properties. In addition, collagens are known to be responsible for the dynamic compressive properties of cartilage [15, 16].

Interstitial fluid contributes 60 - 87% of the cartilage weight. The remaining 13 - 40% consists of type II collagens (60 - 80%), PGs (20 - 40%), glycoproteins and non-collagenous proteins (15 - 20%) [27, 67, 116].

2.2 Organization of the tissue

Structure of the articular cartilage is highly anisotropic (Figures 2.1B and 2.2) and, thus, its mechanical properties are strongly dependent on direction. Articular cartilage may be divided into four major zones (or layers) which are superficial, middle, deep and calcified cartilage (Figure 2.1B) [67, 70, 116, 137]. In the superficial zone, the chondrocytes are small, flat and arranged tangentially to the articular surface [137, 156]. In the superficial zone, the cartilage PG content [79] and collagen volume density [71] are lowest, the water content is highest [67] and the collagen fibrils are arranged in parallel to the articular surface [19, 38, 137]. In the intermediate zone, the chondrocytes are moderate in size and spherical in shape [137, 156]. The tissue PG content [79], collagen volume density [71] and water content [67] are moderate and the collagen fibrils are randomly oriented [19, 38, 137]. The largest and metabolically most active chondrocytes, arranged in vertical columns, are found in the deep zone [40, 137, 156]. In the deep zone, cartilage PG content and collagen volume density are highest [71, 79], the water content is lowest [26, 67] and the collagen fibrils are arranged radially [19, 38, 137]. The calcified zone is calcified with crystals of calcium salts and the chondrocytes are smaller than those in the deep zone. Collagen fibrils penetrate from the deep zone directly through calcified cartilage into subchondral bone [26].

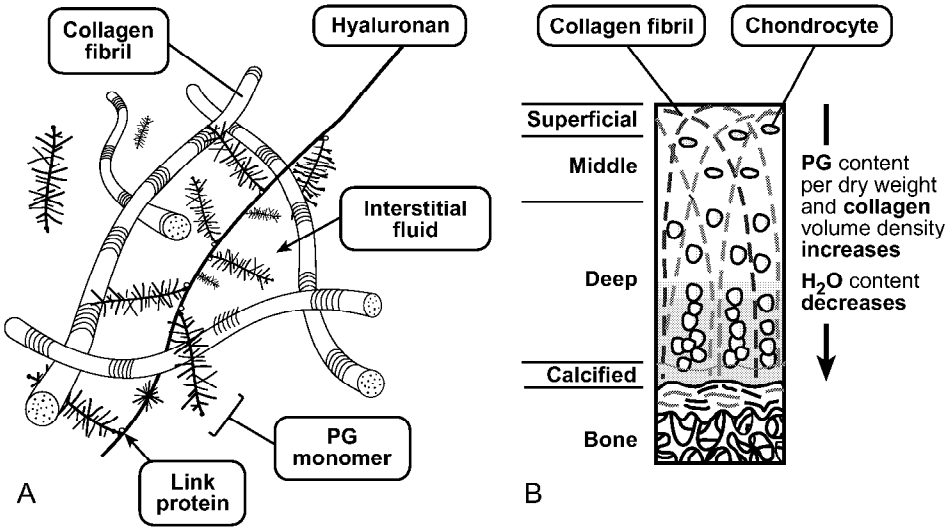

Figure 2.1: (A) Schematic representation of the three dimensional arrangement of collagen fibrils and proteoglycan macromolecules in cartilage. The proteoglycan aggregate consists of proteoglycan monomers which are attached to hyaluronan (hyaluronic acic) acid by a link protein. The proteoglycan monomer consists of repeating units of negatively charged glycosaminoglycan side chains attached to protein backbone [116]. (B) Cartilage tissue may be divided depth-wise into four different zones (superficial, middle, deep and calcified cartilage) in which cartilage structure, composition and mechanical properties differ [19, 67, 70, 71, 116, 137].

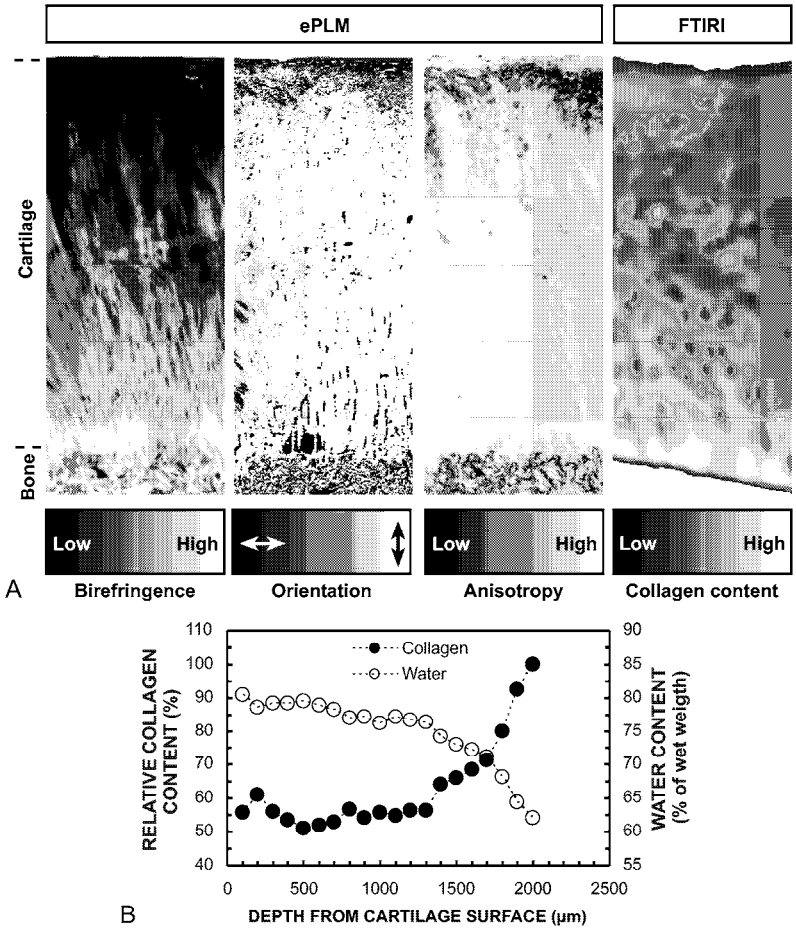

Figure 2.2: (A) Microscopic images of human patellar articular cartilage, as obtained using enhanced polarized light microscopy (ePLM) [138] and Fourier transform infrared imaging (FTIRI) technique [140]. In the ePLM, internal orientation and anisotropy of the tissue may be calculated (utilizing Stokes's equations) [138]. In the superficial zone collagen fibrils are arranged in parallel to the articular surface, in the middle zone collagens are randomly organized, whereas in the deep, zone collagen fibrils are arranged radially. In the FTIRI, integrated absorbance of amide I and II peaks may be used for the determination of cartilage collagen content. (B) Collagen concentration increases with increasing distance from the joint surface (and also from the chondrocyte [71]), whereas water content decreases towards the cartilage-bone junction (for calculation of water content, it was assumed that solid matrix is 1/3 of proteoglycans and 2/3 of collagen [140]).

CHAPTER III

Osteoarthrosis and cartilage injuries

"From Hippocrates down to the present age, we shall find that an ulcerated cartilage is universally allowed to be a very troublesome disease and that, when destroyed, it is never recovered". This quote from W. Hunter (1743) [76] is still topical since articular cartilage has a very limited capability for self-repair.

3.1 Pathogenesis of osteoarthrosis

Metabolic disease processes and mechanical injuries are the major mechanisms which lead to degenerative joint disease and cartilage degeneration [70]. Degenerative joint diseases have a strong association with age and they are more common in women. In addition, overweight, heavy and long-term physical work, as well as genetic susceptibility associate with the degenerative joint diseases [27]. In rheumatoid arthritis, the inflamed synovium drives the degradation of the articular cartilage. However, in OA cartilage degradation is mostly driven by chondrocytes [53]. The early osteoarthrotic changes include an increase of the cartilage water content, depletion of the superficial PGs, degradation of the collagen fibril network [10, 27, 116], increase of cartilage permeability and decrease of cartilage stiffness [8, 90, 131]. The degeneration of the collagen network is especially harmful to cartilage [26, 27], since the turnover time of the collagens is more than several decades [17]. In OA, the increased water content and swelling of the tissue may be primarily related to disruption of collagen fibrils [18]. Only after severe structural and compositional changes in the tissue, may the first visual signs of cartilage degeneration be detected. Cartilage degeneration may be divided into the following clinically detectable phases [26, 27]:

- In the first phase, fibrillation and small fissures of the cartilage surface occur. In the underlying bone, a minor sclerosis (increase of density) may be revealed. The increased density of the subchondral bone results from formation of new layers of bone on existing trabeculae. In the radiographic image, subchondral sclerosis and minimal narrowing of joint space may be seen.

- In the advanced phase of degeneration, free fragments of cartilage are released into the joint space from the superficial tissue and the fissures of the tissue penetrate to subchondral bone. These changes decrease cartilage thickness and lead to significant narrowing of the joint space. In the advanced phase, subchondral bone sclerosis is pronounced and osteophytes are formed. Joint space narrowing and subchondral sclerosis are now clearly seen in the radiographic image.

- In the end-stage of degeneration, the progressive loss of articular cartilage takes place and subchondral bone is exposed. Subchondral cysts and capsular fibrosis may be seen.

It is not clear which is the initiating process - structural changes and softening in articular cartilage or, alternatively, sclerosis and stiffening of the underlying bone. Impairment of cartilage functional properties causes bone-remodeling due to increased peak stresses on the subchondral bone. On the other hand, bone stiffening increases stress on the overlying cartilage. In most cases, cartilage degeneration and remodeling of subchondral bone are both present when the symptoms become apparent [27].

Clinically, degenerative joint disease is usually characterized by pain, joint stiffness and loss of mobility [27]. At this point, cartilage degeneration is usually in the advanced phase. Articular cartilage lacks neural elements but the subchondral bone and the soft tissues of the knee joint (such as synovium, joint capsule and ligaments) are innervated. In the knee, the nociceptors consist of free nerve endings, which may be sensitized and activated mechanically and chemically by injuries and inflammation, respectively [162]. Thus, cartilage lesions that involve the subchondral bone or irritate the synovium give rise to the pain that is typically related to cartilage injuries.

When medical therapy fails to relieve the pain related to the OA of the knee, arthroscopic débridement of the articular surface or lavage of the joint is often recommended. However, in a controlled trial, the outcome after arthroscopic lavage or débridement was equal to that of a placebo procedure [115]. Furthermore, in the study of Kalunian et al. [84], both treatment and control groups reported improvements in function at 12 months and there was no statistically significant difference between the groups during the follow-up. It can be concluded that despite their current popularity, lavage and débridement may not be particularly efficacious for most individuals with knee OA [50, 147].

3.2 Diagnosis of osteoarthrosis

Currently, the diagnostics of OA is based on the clinical investigation, radiography, qualitative MRI analysis or visual evaluation and palpation of the articular surface

during arthroscopy. Radiographic imaging is used for revealing the joint space narrowing and the subchondral sclerosis. Direct visualization during arthroscopy does not allow imaging of the internal cartilage structure, limiting the amount of diagnostic information. It is obvious that current diagnostic techniques are insensitive at detecting the earliest signs of cartilage degeneration. In addition, the progress of surgical treatments of osteochondral injuries has created a need for improvements in diagnostic and monitoring techniques.

MRI is the most promising non-invasive method to detect changes in cartilage structure and composition [29, 127, 125, 171]. T_2 relaxation time is a sensitive parameter for detecting the integrity of the cartilage collagen network [125, 171]. The PG content of the tissue may be estimated by the measurement of T_1 in the presence of the negatively charged gadolinium-diethylenetriaminepentaacetic -acid ($Gd\text{-}DTPA^{2-}$) as a paramagnetic contrast agent [127]. It is assumed that the contrast agent molecules distribute into cartilage in an inverse relation to negatively charged GAGs. However, resolution of the low-field (< 2 T) clinical MRI devices is, at its best, hundreds of micrometers, which does not permit the detection of superficial cartilage fibrillation and depletion of superficial PGs. Furthermore, MRI does not provide a means for direct measurement of the functional properties of cartilage, although the high-field (9.4 T) MRI has been used successfully to predict indirectly cartilage stiffness *in vitro* [126].

In optical coherence tomography (OCT, or "optical biopsy") [72, 75], the intensity of the back scattered infrared light is measured somewhat analogously to B-mode ultrasound imaging. OCT provides typically 5 - 15 μm imaging resolution, which is better than that of any available clinical technology. The instrumentation of the OCT is relatively low cost and due to optical fiber based probing, the technique can be easily integrated into clinical arthroscopic units. The main limitation of the OCT is that it does not provide any direct information of the cartilage functional properties and the penetration of the infrared light into tissue below the cartilage surface is limited.

Electromechanical techniques [55, 105, 145], based on the measurement of streaming potentials induced by compression, are now in preclinical development and can detect cartilage degeneration, being especially sensitive to depletion of tissue PGs. Electromechanical techniques, however, do not enable measurement of the cartilage thickness or high resolution imaging of the tissue. Furthermore, when using a constant indenter diameter and tissue deformation, tissue thickness can modify the fluid flow. Therefore, the unknown tissue thickness may jeopardize the reliability of the streaming potential measurement.

Traditionally, the functional properties of articular cartilage have been characterized using mechanical indentation measurements *in situ* and a number of indentation instruments have been introduced for arthroscopic evaluation of cartilage [7, 13, 41, 108, 123]. Although none of these indentation instruments is capable of

measuring tissue thickness, a factor which affects the results especially when thin tissue is indented [69, 111, 175], these instruments may increase significantly the diagnostic information obtainable during arthroscopy. By using an arthroscopic indentation instrument, it has been shown, that patients with chondromalacia patella in general suffer softening in the knee joint cartilage, although visible cartilage degeneration is localized only in the patella [107]. Earlier, Dashefsky (1987) [41] revealed with a microminiature pressure transducer, that visually intact cartilage surface areas were softer in patients with chondromalacia patella, as compared to controls.

In the ultrasound indentation technique, the ultrasound transducer is used as an indenter and the tissue thickness and deformation are calculated from the ultrasound signal during the compression [85, 159, 177]. This technique enables an objective calculation of the tissue material parameters, provided that the sound speed in the cartilage is known and a valid model of cartilage mechanics is used for the calculation of parameters. The *in situ* calibration method, which was presented by Suh et al. (2001) [159], enables also the determination of the sound speed. However, the apparent complexity of the instrumentation may limit its clinical use. With enhanced ultrasound techniques, cartilage surface roughness and fibrillation [2, 34, 35, 36, 37, 46], as well as osteoarthrotic changes in the subchondral bone [146], have been determined. However, the detection of the cartilage surface roughness by measuring backscattered ultrasound signal in many different angles between the transducer and articular surface [2, 34, 35] may be technically difficult to undertake *in vivo*. In a recent study, Disler et al. (2000) [46] successfully used qualitative ultrasound methods for detecting and grading knee OA *in vitro*.

3.3 Cartilage repair techniques

When the cartilage degeneration has reached the end-stage, the common procedure is the installation of an endoprothesis. If the cartilage injury is local, surgical repair techniques may be used for treating the damage. Articular cartilage lesions are common after joint trauma and they can be confined to the cartilage layer or penetrate the cartilage and reach the subchondral bone. The popularity of different sports activities has led to an exponential increase in cartilagineus injuries [31]. Current research on cartilage repair is now focusing on the use of gene therapy and tissue engineering techniques. Cartilage repair techniques may be divided into intrinsic and extrinsic types. In the extrinsic type of repair, the surgeon introduces active biological compounds in the injured cartilage area to induce cartilage regeneration. In the intrinsic repair, the cartilage is stimulated to heal via its own spontaneous repair mechanisms [70].

Mosaicplasty [64, 65] and ACT [22, 23] (Figure 3.1) are the most common techniques of extrinsic repair of cartilage and underlying bone. In mosaicplasty, cylindrical osteochondral autografts are harvested from the non-weight-bearing regions

of the patello-femoral joint and used for filling the pre-drilled holes in the defect site. The advantages of this technique are that the grafts have the composition and structure of hyaline cartilage, it is one-step procedure and can be performed arthroscopically [162]. Autografts are immunocompatible, but the harvesting can cause problems in the donor site and the size of the treated lesion is limited (6 - 8 cm^2). The use of osteochondral allografts [57], which are available from donors, does not require the harvesting of the cartilage from the individual's own joint. However, the allografts may provoke an immunological response and can theoretically transmit infections.

The ACT procedure [22, 23] has two distinct phases (Figure 3.1). According to Brittberg et al. (1994,1999), in the first phase, articular cartilage is harvested from the non-weight-bearing areas of the lateral femoral condyle, chondrocytes are isolated enzymatically from the cartilage sample, and the number of chondrocytes is multiplied in cell culture for 14 days. In the second phase, a periosteal flap is sutured over the defect site and the chondrocytes are injected under the periosteum [23]. The biological repair process after ACT is still not well characterized and, therefore, it would be essential to characterize quantitatively the repair tissue and the subchondral bone preferably both from animal models and from human patients.

Poor integration of the repair tissue with the surrounding cartilage, as well as the possible loss of periosteal flaps in the ACT repaired knee, hinder restoration of mechanical competence of articular cartilage during the healing process. Thus, it would be desirable to use post-operative biomechanical measurements to follow healing *e.g.* after mosaicplasty or ACT [61, 77]. In a previous study, Vasara et al. (2002) proposed that mechanical measurements were able to indicate incomplete mechanical maturation of the cartilage, even though the biochemical composition of the repair tissue (PG content) had been largely restored after ACT-surgery [163]. On the other hand, high resolution *in vivo* imaging techniques could provide a means to monitor the structural maturation of the tissue and also delineation of the repair area before the operation [77].

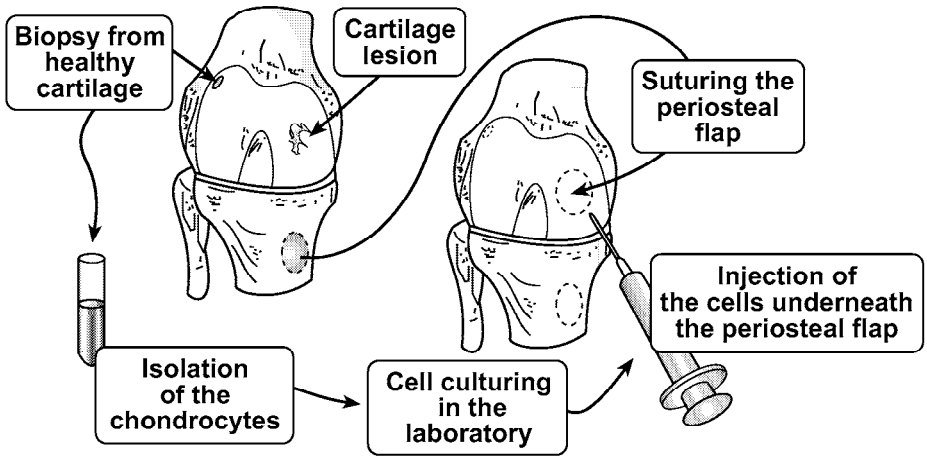

Figure 3.1: Schematic representation of the autologous chondrocyte transplantation procedure [22, 23]. In the first phase, biopsy of healthy cartilage is taken from the non-weight bearing area of the joint. Subsequently, chondrocytes are isolated from the cartilage sample and the number of chondrocytes is multiplied in the cell culture for several weeks. Finally, a flap of periosteum is sutured over the lesion site and the autologous chondrocytes are injected underneath the periosteum.

CHAPTER IV

Mechanical properties of articular cartilage

During joint loading, cartilage deforms to increase contact areas and to improve local joint congruence [116]. Furthermore, the response of the tissue to an applied load varies with time. Creep and stress relaxation are manifestations of the viscoelastic behavior of articular cartilage.

4.1 Measurement techniques

In a *creep test*, the application of a step force results in a time-dependent increase of deformation of the tissue. In a *stress-relaxation test*, a constant displacement is applied instantaneously or at a constant strain rate. This displacement results initially in a stress-rise followed by a period of stress decrease until an equilibrium state is reached. At *equilibrium*, no fluid flow or pressure gradients exist, and the load is therefore controlled only by the solid matrix. After removal of the load or the deformation, cartilage will recover its initial dimensions at a rate controlled by the material properties.

The mechanical properties of articular cartilage are most frequently determined by using unconfined compression, confined compression or indentation tests [118]. For unconfined and confined compression, the cartilage sample (usually cylindrical) must be isolated from the subchondral bone and, therefore, these geometries are suitable only for *in vitro* testing. In *confined compression*, a cartilage sample is inserted into a confining chamber and the other sample surface is compressed with a porous, *i.e.* permeable piston (both bottom and the walls of the chamber are impervious, *i.e.* non-porous). During confined compression, the fluid may flow freely only via the porous piston and, thus, the problem is mathematically one-dimensional. In *unconfined compression*, a cartilage sample is compressed between two smooth impervious (metallic or glass) platens and expansion and fluid flow are allowed only in the lateral direction. In the *indentation test*, cartilage is compressed with a plane-ended (or spherical-ended) indenter and the method can be applied for

in situ testing of cartilage. The indenter may be permeable or impervious. Both the stress-relaxation and creep test can be applied in all of these geometries.

4.2 Theoretical models of articular cartilage mechanics

The mechanical behavior of articular cartilage may be described by using analytical or numerical models. For simple geometries, most cartilage models may be solved analytically. In complex geometries, such as in real joints, a numerical analysis is required [67]. Further, the complex nonlinear behavior of cartilage, as well as structural and mechanical anisotropy, can be modeled most realistically using the finite-element (FE) analysis. In the earliest model of articular cartilage, the tissue was modeled as linearly elastic, single phasic, isotropic and homogeneous material. In that model, deformation was assumed to be infinitesimal and the contact between the cartilage and compressive platen was set to be frictionless. For an elastic material that is compressed in unconfined geometry, Young's modulus is determined as the ratio of axial stress (σ) and strain (ϵ):

$$E = \frac{\sigma}{\epsilon}. \tag{4.1}$$

This equation is commonly known as a generalization of the Hooke's law. Based on the assumption of material isotropy, the aggregate modulus (H_a), *i.e.* the equilibrium modulus in confined compression, is related to E and Poisson's ratio (ν) [82, 118]:

$$H_a = \frac{(1-\nu)}{(1+\nu)(1-2\nu)}E. \tag{4.2}$$

Single phasic elastic model for indentation geometry

The first realistic model for indentation geometry was introduced by Hayes et al. during the early seventies [69]. Hayes et al. (1972) assumed cartilage to be an elastic material, bonded to a rigid underlying solid material. The strain was assumed to be infinitesimal and the contact between the indenter and cartilage was set to be frictionless. Boundary conditions for the plane-ended (porous) indenter (radius = a) lying on the cartilage surface ($z = 0$) and for the cartilage-bone interface ($z = h$) are in the cylinder coordinates (r, θ, z)

$$\begin{array}{ll} u_z = \omega_0 & 0 \leq r \leq a, z = 0 \\ \sigma_{zz} = 0 & a < r < \infty, z = 0 \\ \sigma_{rz} = 0 & 0 \leq r < \infty, z = 0 \\ u_r = u_z = 0 & 0 \leq r < \infty, z = h \end{array} \tag{4.3}$$

where $(u_r, 0, u_z)$ are components of the displacement vector in cylinder coordinates, σ_{zz} and σ_{rz} are normal and tangential stress components, respectively. Elastic displacement is ω_0 $(= \epsilon h)$ in z-axis under the indenter $(r = 0)$. Generally, this axial symmetric contact problem is solved by expressing the strain vectors in a form of Boussinesq-Papkovitz potential functions. In this way, the expression follows Fredholm's second order integral, which gives the expression for the Young's modulus:

$$E = \frac{\sigma}{\epsilon}\frac{\pi a}{(2h\kappa)}(1-\nu^2), \tag{4.4}$$

where $\kappa(a/h, \nu)$ is a theoretical scale factor that accounts for the variable cartilage thickness (h) [69]. During the instantaneous and equilibrium phases of the compression tissue behaves like an elastic solid material (no fluid flow) and the Young's modulus may be calculated using the equation (4.4). Under infinitesimal instantaneous compression, the cartilage may be assumed to be incompressible, *i.e.* Poisson's ratio is 0.5 [111, 170], and the dynamic modulus may be determined objectively. For calculation of the Young's (equilibrium) modulus, the true value of Poisson's ratio of the solid matrix must be used [111]. However, if the Poisson's ratio is assumed or determined incorrectly for the equilibrium state, relatively large errors may result in the determined modulus values.

In the nonlinear isotropic elastic FE model, the values of κ have been calculated also for finite deformations [175]. The factor κ increases almost proportionally to the increase of the indentation depth, especially with large Poisson's ratio and aspect ratio values. In our previous study, indentation tests using the single phasic elastic model [69] showed significantly higher equilibrium Young's modulus values than those obtained from the unconfined and confined tests [97]. When the κ values for finite deformations [175] were used, the Young's moduli of the indentation were slightly lower (<11%), but still significantly higher than values from the unconfined and confined compression tests [99]. This discrepancy may be explained by the findings that the indentation response of the cartilage is strongly influenced by thickness and the high tensile stiffness of the superficial fibrillar network [95, 97], which is not taken into account in the isotropic elastic model.

Viscoelastic theory

Single phasic elastic model cannot be applied to characterization of the time-dependent behavior of cartilage. Generally, the time-dependent response of the viscoelastic material may be described as a combination of linear springs (elastic response, Hookean body) and dashpots (viscous response, Newtonian body). In the Maxwell and Kelvin-Voigt models, the spring and dashpot are connected in series and in parallel, respectively. Parsons and Black (1977) introduced a viscoelastic model of cartilage [133] in which the viscoelastic creep response of the tissue was explained

by using the generalized Kelvin solid model. In the generalized Kelvin solid, one spring and several Kelvin-Voigt pairs are connected in series. Under a stepload, the linear spring represents the instantaneous elastic response and the Kelvin-Voigt pairs represent the time-dependent creep. The time (t) dependent creep compliance ($J(t)$) is defined as follows:

$$J(t) = J_u + \sum_i J_i(1 - e^{-t/\tau_i}), \tag{4.5}$$

where J_u ($= 1/E_u$) is the unrelaxed shear compliance, J_i is relaxed shear compliance of the i^{th} element and τ_i is the retardation time of the i^{th} element. The study of Parson and Black (1977) extended the single phasic elastic model [69] and proposed that the time-dependent creep rate of articular cartilage can be described in terms of continuous retardation time spectrum, that can be approximated by the slope of logarithmic time vs. compliance (strain/stress) curve

$$k(t) = \frac{\mathrm{d}(J(t))}{\mathrm{d}\ln t}, \tag{4.6}$$

which is the slope of a creep compliance $J(t)$ against $\ln t$ [133]. For rabbit cartilage, Parsons and Black (1977) found k to be nearly constant over a wide time scale (1 - 1000 s). In articular cartilage k is a structural parameter which depends on the indenter size, material properties and thickness of the tissue. Therefore, these factors should be taken into account when interpreting creep measurements of the cartilage.

Dynamic modulus of cartilage is determined to observe the response of the tissue to a cyclic deformation at a particular frequency [68, 103]. The dynamic modulus (E_{dyn}) for a viscoelastic material is complex in nature:

$$E_{dyn} = E_1 + iE_2, \tag{4.7}$$

where E_1 is the storage modulus, proportional to the elastically stored energy, and E_2 is the loss modulus, describing the viscous energy dissipated in the loading process. Typically the absolute value of the E_{dyn} is presented:

$$|E_{dyn}| = \sqrt{{E_1}^2 + {E_2}^2} = \frac{\sigma}{\epsilon}, \tag{4.8}$$

where σ is now the dynamic stress exerted on the sample and ϵ is the strain. Due to the viscoelasticity of the cartilage, the dynamic modulus of cartilage depends on the test frequency and is typically several times the equilibrium modulus [30]. However, in indentation geometry Quenneville et al. (2003) [135] demonstrated that the peak load of the cartilage becomes constant (*i.e.* tissue behaves like elastic material) when the compressive ramp velocity is over 500 μm/s.

Biphasic model

Movement of the interstitial fluid has a fundamental role in the viscoelastic behavior of cartilage tissue. Therefore, a realistic model of cartilage should include at least two phases; a solid and a fluid phase. In the linear biphasic theory [119] the solid phase consists of the collagen-PG-matrix and the fluid phase consists of the interstitial water. This model is called linear because the permeability is assumed to be independent of the level of tissue deformation and the solid phase is mechanically linearly elastic.

In the model, both solid and fluid phases are assumed to be incompressible. The solid matrix is porous, homogeneous and isotropic, whereas the fluid phase is inviscid. The total stress acting on cartilage is the sum of the stresses acting on the solid phase and fluid phase. At equilibrium, the entire load is carried by the solid matrix. Continuity equation of the biphasic model is:

$$\bigtriangledown \cdot (\phi^s \mathbf{v}^s + \phi^f \mathbf{v}^f) = 0, \tag{4.9}$$

where ϕ^s and ϕ^f are solid (s) and fluid (f) volume fractions, respectively, and $\mathbf{v}^s$ and $\mathbf{v}^f$ are solid and fluid velocity vectors, respectively. Momentum equations are:

$$\bigtriangledown \cdot \ \boldsymbol{\sigma}^\alpha + \boldsymbol{\pi}^\alpha = 0, \tag{4.10}$$

$$\boldsymbol{\pi}^s = -\boldsymbol{\pi}^f = \frac{(\phi^f)^2}{k_p}(\mathbf{v}^f - \mathbf{v}^s), \tag{4.11}$$

where $\alpha = s, f$ and $\boldsymbol{\sigma}^\alpha$ is (solid or fluid) stress tensor, $\boldsymbol{\pi}^\alpha$ is diffuse (solid or fluid) body force vector (*i.e.* the rate of momentum transfer to the solid or fluid phase) and k_p is permeability. Constitutive equations are:

$$\boldsymbol{\sigma}^f = -\phi^f p\mathbf{I}, \tag{4.12}$$

$$\boldsymbol{\sigma}^s = -\phi^s p_h \mathbf{I} + \tilde{\boldsymbol{\sigma}}^s, \tag{4.13}$$

$$\boldsymbol{\sigma}^t = \boldsymbol{\sigma}^s + \boldsymbol{\sigma}^f, \tag{4.14}$$

where p_h is hydrostatic pressure, $\mathbf{I}$ is unity tensor, $\tilde{\boldsymbol{\sigma}}^s$ is the effective solid stress tensor (represents the portion of the solid stress that is in excess of the local fluid pressure) and $\boldsymbol{\sigma}^t$ is the total stress tensor.

In the linear biphasic poroelastic model, the solid matrix is assumed to be linearly elastic. Following linear elasticity ($\tilde{\boldsymbol{\sigma}}^s$) can be expressed as:

$$\tilde{\boldsymbol{\sigma}}^s = B_s \mathrm{trace}(\boldsymbol{\epsilon}^s)\mathbf{I} + 2\mu_s \boldsymbol{e}^s, \tag{4.15}$$

where B_s is elastic bulk modulus, trace is a sum of the diagonal elements of the given matrix, $\boldsymbol{\epsilon}^s$ is solid strain tensor, μ_s is elastic shear modulus and $\boldsymbol{e}^s$ is deviatoric component of the solid strain tensor ($= \boldsymbol{\epsilon}^s - 1/3\mathrm{trace}(\boldsymbol{\epsilon}^s)\mathbf{I}$) [45]. Linear biphasic theory has been applied succesfully for the analysis of cartilage compression measurements in numerous studies.

Other models

The linear biphasic model has been used successfully to predict quasi-static tests, but it has failed to predict dynamic compressive behavior in unconfined compression [24, 39, 44] or indentation [54]. To overcome these problems, further development of the original biphasic model [119] has continued. In the biphasic poroviscoelastic theory [110], the apparent viscoelastic behavior of cartilage is ascribed to intrinsic viscoelasticity of the collagen-PG-matrix together with the interstitial fluid flow. This provides a means to assess the relative significance of each mechanism and, obviously, this also improves the ability of the model to predict the dynamic stiffness of the tissue [45, 43]. The biphasic poroviscoelastic model is able to capture cartilage stress-relaxation in unconfined and unconfined compression and indentation [43] significantly better than the linear biphasic model.

In the triphasic model [101], an ion phase was included in the biphasic model. With the triphasic constitutive laws [101], stresses, strains, ion concentrations, electric and flow fields within a layer of charged hydrated soft tissue of finite thickness can be calculated [58, 59, 60, 120, 101].

In the linear transversely isotropic biphasic model, material properties can be defined separately in the transverse plane and in the out-of-plane (altogether five elastic constants and one [169] or two [39] permeability coefficients). Similarly to the biphasic poroviscoelastic model [110], the transversely isotropic biphasic model predicts [39] the cartilage dynamic response better than the original biphasic isotropic model [119]. However, the transversely isotropic model cannnot simultaneously describe the observed equilibrium behavior and stress relaxation of calf cartilage in unconfined and confined compression [28]. By integrating the continuum-based conewise linear elasticity model and biphasic mixture theory as a conewise linear elasticity biphasic solution [154], the agreement of the theory with unconfined and confined compression tests has been more successful and the material parameters have been consistent with the previous reports in the literature. Further, Huang et al. [74] combined the biphasic conewise linear elasticity model [154] with the biphasic poroviscoelastic model [110]. Huang et al. demonstrated that simultaneous prediction of the compression and tension characteristics of cartilage (under unconfined compression) could only be achieved if the compression-tension nonlinearity of the tissue, in addition to the fluid-flow and the intrinsic flow-independent viscoelasticity of the matrix, were taken into account.

Soulhat et al. developed and solved analytically a fibril-reinforced poroelastic model in which the homogenous isotropic biphasic gel is fibril-reinforced (describing the role of the collagen fibrils) [155]. The fibrils were considered to provide stiffness in tension only. The fibril-reinforced poroelastic model offers similar advantages as the conewise linear elastic model [154], incorporating the cartilage compression tension nonlinearity. The description of the collagen fibril-reinforced matrix is the main benefit obtained with the fibril reinforced model [106, 155].

4.3 Mechanical characteristics of articular cartilage

Cartilage thickness and mechanical properties vary between different species and anatomical locations [14, 81, 109, 153] (Table 4.1). Furthermore, the values depend on the measurement direction [83, 98, 164, 165] and geometry (unconfined or confined compression, or indentation test) [97]. In compression tests, the dynamic modulus values are dependent on the testing frequency and the dynamic moduli are typically several times higher than the equilibrium Young's moduli. Typical values of human and bovine cartilage equilibrium Young's modulus, equilibrium aggregate modulus, equilibrium Poisson's ratio and permeability are presented in Table 4.1 (values are determined in axial compression).

The mechanical properties of cartilage vary between cartilage zones [62, 148, 165, 176]. This is a result of the structural and compositional differences between zones. Generally, in an axial direction, compressive stiffness increases [62, 148, 165] and tensile stiffness decreases [4] with increasing distance from the surface. In indentation geometry, in particular the high transverse stiffness and thickness of the superficial zone modifies the cartilage stiffness (especially during dynamic loading) [99].

Typically, cartilage tensile properties are determined for slices that are cut from the different layers (zones) of the tissue and, in the tension test, the samples are extended in the lateral direction [4, 86, 89, 88, 91, 142]. In human femoral condyle cartilage, the typical fracture stress has been proposed to be in the range of 1 - 40 MPa [86, 89, 91, 142]. Akizuki et al. (1986) suggested that for human cartilage the equilibrium tensile stiffness (in the patellar groove or medial condyle) is <30 MPa [4]. Recently, Elliott et al. (2002) reported similar results [49]. It has been proposed that the compressive modulus of bovine humeral cartilage is up to 10 times lower than the tensile modulus [98] in the direction perpendicular to the cartilage surface. The high tensile stiffness of the cartilage is attributable to the tendency of the collagen fibrils to resist tension only [87].

Table 4.1: Typical values of biphasic material parameters of human and bovine articular cartilage in compression as determined by using unconfined and confined compression or indentation tests (Equilibrium Young's modulus (E), equilibrium aggregate modulus (H_a), equilibrium Poisson's ratio (ν) and permeability (k_p)).

Measurement site	H_a **(MPa)**	E **(MPa)**	ν	k_p $\times 10^{-15}$**(m^4/Ns)**
Human cartilage				
Patellar groove [14, 83]	0.5 - 0.9	0.6	0 - 0.16	2.2
Patella [8]	0.9			
Medial condyle [14]	0.6		0.07	1.1
Bovine cartilage				
Patellar groove [14]	0.5		0.25	1.4
Patella [99, 14, 43]	0.6	0.5 - 0.8	0.10 - 0.36	1.7
Medial condyle [99, 14]	0.3 - 0.9	0.3 - 0.6	0.21 - 0.43	0.5

CHAPTER V

Acoustic properties of articular cartilage

5.1 Basics of ultrasonic measurements

By definition, ultrasound frequency is higher than the maximum hearing frequency of the human ear (typically 20 kHz). Ultrasound attenuation, reflection and scattering, as well as speed, depend on the mechanical properties, composition and structure of the material. Therefore, ultrasound is a feasible way to undertake the nondestructive testing of biomaterials. Ultrasound waves are generated and received with ultrasound transducers. Briefly, in an ultrasound transducer, the application of an alternating electric pulse across the piezoelectric crystal changes rapidly thickness of the crystal, generating a progressive pressure wave to the surrounding media. When the sound wave reaches the transducer, sound pressure generates an electric pulse across the crystal.

In general, an ultrasound field can be focused or unfocused (Figure 5.1). An ultrasound field may be focused by using acoustic lenses, reflectors or spherically curved transducers. In addition, the ultrasound field can be electrically focused by transducer arrays, driven with signals having appropriate phase differences (phased array technique) [47, 166, 167]. The distance of the focal point (or the transition point between the near and far fields when using unfocused transducer), as well as the focal beam width and depth, determine the usability of the transducer for the specific task. Basic equations for the ultrasound fields are presented in Table 5.1.

The acoustic interface is defined as an interface between two materials with different acoustic impedances. In pulse echo measurement, ultrasound reflections and backscattering from the acoustic interfaces are measured and from this data, ultrasound reflection and backscattering parameters can be determined. In the through-transmission mode, the transducers are located in the opposite sides of the sample and by measuring the time of flight (TOF, *i.e.* the travel time of the sound through the sample) and amplitude of the received signal, sound speed and attenuation may be determined.

Table 5.1: Basic equations for the ultrasound fields, reflection, refraction, transmission and attenuation [47, 128, 166, 167]. In the equations, $A(0)$ is incident amplitude, a is the radius of the transducer, c is sound speed in the material, f is frequency, $I(0)$ is incident intensity, I_{avg} is spatial average of intensity over the radiating surface, d and e are tissue specific experimental coefficients, R_c is the radius of curvature, λ is the wavelength, ρ is the density of the material, θ is the angle of incidence, reflection or refraction. Subscripts 1 and 2 stand for parameters in material 1 and 2, whereas i, t and r stand for incident, transmitted and reflected waves, respectively.

Parameter	Equation
Intensity at distance x	$I(x) = I(o)\sin^2[(\pi/\lambda)(\sqrt{a^2+x^2}-x)]$ (unfocused field)
Intensity at distance x	$I(x) = I_{avg}([R_c/(R_c-x)]\sin([\pi 4a^2(R_c-x)]/(8\lambda x R_c)))^2$ (spherically curved transducer)
Focal length	$F = R_c/(1-c/c_{lens})$ (lens transducer)
Beam width at focal zone	$B_W = \lambda F/(2a)$ (at -6 dB)
Depth of focal zone	$F_D = 7\lambda[F/(2a)]^2$ (at half maximum intensity)
Acoustic impedance	$Z = c\rho$
Snell's law for reflection	$\theta_i = \theta_r$
Snell's law for refraction	$c_2 \sin\theta_1 = c_1 \sin\theta_2$
Reflection coefficient	$R = I_r/I_i = [(Z_2\cos\theta_1 - Z_1\cos\theta_2)/(Z_2\cos\theta_1 + Z_1\cos\theta_2)]^2$
Transmission coefficient	$T = I_t/I_i = 4Z_1Z_2\cos\theta_1\cos\theta_2/(Z_2\cos\theta_1 - Z_1\cos\theta_2)^2$
Amplitude at distance x	$A(x) = A(0)\mathrm{e}^{-\alpha x}$ (attenuation)
Attenuation coefficient	$\alpha = df^e$

5.2 Acoustic characteristics of articular cartilage

The published literature indicates that degeneration of the articular cartilage may be detected as a change in the acoustic characteristics of the tissue [36, 78, 121, 124, 159, 161]. According to previous studies, the sound speed decreases in degenerated tissue, as compared to intact tissue [78, 121, 124, 159, 161]. After specific, enzymatic degradation of the collagen network [161] and PGs [124] a minor but significant decrease in the sound speed has been revealed. Results regarding the interrelationships between the speed of sound and cartilage PG content are, however, somewhat conflicting [124, 159, 161]. Furthermore, Agemura et al. (1990) proposed that collagen fibril orientation may affect the sound speed [3]. Traditionally, the ultrasound pulse-echo technique has been proposed to be a reliable method for the detection of cartilage thickness [1, 104, 114, 143, 159, 161]. However, a major site-

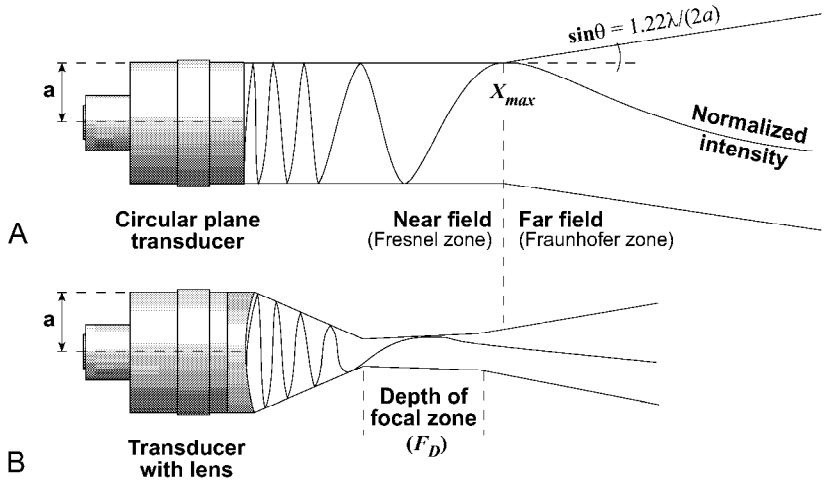

Figure 5.1: Demonstration of the (A) unfocused and (B) focused ultrasound fields. In the unfocused field, the last axial intensity maximum occurs at the distance $X_{max} = (4a^2 - \lambda^2)/4\lambda \approx a^2/\lambda$ when a is $\gg \lambda$. Ultrasound must be focused in the near field of an equivalent plane transducer. Basic equations for the ultrasound fields are presented in Table 5.1.

dependent variation in the (human) cartilage sound speed (1419 - 2428 m/s) was recently reported by Yao and Seedhom (1999) [173]. Although their study may have methodological limitations [113], the possible site dependent variation in the sound speed may jeopardize the accuracy of the ultrasonic measurement of articular cartilage thickness and, therefore, this issue should be further investigated.

Frequency dependent attenuation induces pulse distortion, which can influence the recorded flight time (TOF) (and sound speed) [122, 136]. Ragozzino (1981) concluded that the effect of the frequency dependent attenuation on the pulse transition time is probably minor compared to the biological variation of sound speed [136]. However, in the previous studies, different methods, such as the cross-correlation technique and detection of the predetermined amplitude point or threshold [32, 33, 130, 136, 157], have been introduced for the optimal determination of the pulse arrival time.

In normal cartilage, attenuation values systematically increase as a function of frequency (at 10 - 100 MHz) [3, 78, 124, 150]. This indicates that there is a significant frequency-dependence of the attenuation in cartilage, as confirmed recently by Joiner et al. (2001) [78] (Table 5.2). Inter-relationship between the frequency

dependent attenuation and cartilage composition and structure is not well characterized. Earlier, Senzig et al. (1992) proposed that the ultrasound attenuation is strongest in the cartilage areas which are under high stresses during joint motion [150]. In enzymatically degraded cartilage, an increase in the ultrasound attenuation has been detected [3, 78, 124] and, thus, the attenuation parameters could be useful for detecting osteoarthrotic changes in the cartilage. Due to the somewhat conflicting results of the previous studies [3, 78, 124, 150], the roles of the PGs and collagens as the determinants of attenuation are not yet clear.

By using a typical sound speed in cartilage (1630 m/s, study IV) and the proposed cartilage density value ($\sim$ 1050 kg/m^3) [80], the acoustic impedance of the cartilage may be approximated to be 1.7×10^6 kg/m^{2}s. However, due to the inhomogeneous and anisotropic structure of cartilage, acoustic impedance may vary as a function of cartilage depth. The ultrasound reflection coefficient (Table 5.2) from the cartilage surface has been shown to be specifically sensitive for the degradation of cartilage superficial collagen [124, 161], but not to be related to any decrease in the cartilage superficial PG content [124, 134, 161]. Chérin et al. (2001) have demonstrated that the integrated reflection coefficient (IRC) and especially the apparent integrated backscatter (AIB), which is related to the backscattering from the internal tissue, correlate with rat age [37]. Both IRC and AIB were suggested to be suitable for the detection of OA in rats [36]. In the previous studies, internal tissue of porcine [93] and rat cartilage [36, 37] has been found to be more echogenic than the human [121] or bovine cartilage [124, 161].

Table 5.2: Summary of the acoustic characteristics of articular cartilage. The values are based on the normal human [78, 121], bovine [3, 124, 150, 159, 161] and rat [36, 37, 134] articular cartilage.

Species and parameter	Range
Human cartilage	
Sound speed [78, 121]	1658 - 1666 (m/s)
Attenuation at 30 Mhz [78]	6.2 - 7.1 (dB/mm)
Frequency dependent attenuation [78]	$0.059f^{1.37}$ - $0.112f^{1.23}$ (dB/mmMHz$^{\gamma}$)
Bovine cartilage	
Sound speed [124, 159, 161]	1634 - 1735 (m/s)
Attenuation at 10 - 40 MHz [150]	2.8 - 6.5 (dB/mm)
Attenuation at 100 MHz [3]	92 - 147 (dB/mm)
Ultrasound reflection coefficient [124, 161]	2.1 - 2.8 (%)
Rat cartilage	
Integrated reflection coefficient [36, 37, 134]	-21 - (-24) (dB)
Apparent integrated backscatter at 50 - 55 MHz [36, 37, 134]	-38 - (-52) (dB)

Chapter VI

Aims of the present study

Previous studies suggest that mechanical and acoustic techniques can provide information about structure, composition and functional properties of articular cartilage. The present *in vitro* and *in situ* studies with bovine and porcine articular cartilage particularly aimed to:

1. investigate the structure-function relationships in cartilage by using selective enzymatic degradations and to describe the site-dependence of the biomechanical properties of cartilage in the bovine knee,

2. combine mechanical and acoustic measurements, in the creation of a novel ultrasound indentation instrument, and to investigate the effects of selective enzymatic degradation on the acoustic parameters, as well as dynamic and time-dependent biomechanical properties of articular cartilage,

3. study the applicability of ultrasound indentation for quantifying site-dependence of the mechanical and acoustic properties of bovine knee articular cartilage *in situ*,

4. clarify the interrelationships between the sound speed and cartilage composition, mechanical properties or degenerative state and to analyze the effect of variation of the sound speed on the reliability of the ultrasound indentation measurements,

5. investigate the ability of ultrasound imaging and quantitative mechanical measurements to diagnose cartilage degeneration and tissue healing after surgical repair of porcine articular cartilage.

CHAPTER VII

Materials and Methods

The present work consists of five studies (I - V), supplemented with unpublished data. The materials and methods used in the studies are summarized in this section. The study design is presented in Table 7.1.

7.1 Elastomer samples

Elastomer samples of varying thickness (0.5 - 6.0 mm, 60° shore A, J-Flex Rubber Products, Redford, Notts, England, $n = 8$) and of different stiffness (1.48 - 17.41 MPa, Teknikum Oy, Vammala, Finland, $n = 13$) were used for initial experimental tests with the ultrasound indentation instrument (II). To simulate the osteochondral structure, elastomer samples were glued with cyanoacrylate on a metal plate.

7.2 Bovine articular cartilage samples

All bovine knee, ankle and humeral joints were obtained from a local slaughterhouse (Atria Oyj, Kuopio, Finland) (I - V). The joints were prepared within five hours *post mortem* (I, II, IV, V) or after storage overnight in the refrigerator (I, III, IV). *Osteochondral blocks* (III) were prepared from the joints using a bandsaw. *Cylindrical osteochondral specimens* (II) were prepared using a hollow drill bit and an autopsy saw (Stryker Autopsy Saw 868, Stryker Europe bv, Uden, The Netherlands). All cylindrical, *full thickness cartilage samples* were detached from the osteochondral blocks (I, II, III and IV) or specimens (II) using a razor blade and a biopsy punch (inner diameter 2 - 4 mm). All unconfined compression tests and the sound speed measurements of the full thickness cartilage samples were conducted with a mechano-acoustic material testing device (section 7.7.1). A mechano-optical device was used for the determination of the Poisson's ratio (section 7.7.1). The measurement sites in the knee and ankle are presented in the Figure 7.1 and the mechanical testing methods are presented in the Table 7.1, respectively.

Table 7.1: Materials and methods used in the studies I - V. All articular cartilage material, if not referred otherwise, was obtained from the bovine knee, ankle or humerus. For measurement sites in the knee and ankle, please, see Figure 7.1.

Study	Cartilage samples	n	Methods	Parameters
I	Five sites at the knee (FMC, LPG, MPG, MTP, PAT)	29	Unconfined compression Poisson's ratio measurement	E_{dyn}, E ν
	Patellar cartilage, before and after enzymatic degradation	18	Unconfined compression	E_{dyn}, E
	Patellar cartilage, cut depth-wise into ten slices	1	Unconfined compression Poisson's ratio measurement DD and PLM microscopy	E ν OD, BF
	Humeral cartilage	1	Unconfined compression and tension tests, FE analysis	E
II	Patellar cartilage, before and after enzymatic degradation	18	Ultrasound indentation Sound speed measurement	E_{dyn}, k, R c
III	Three sites at the knee (FMC, MTP, PAT)	18	Unconfined compression Ultrasound indentation DD microscopy	E_{dyn}, E E_{dyn}, R OD
IV	Four sites at the knee (FMC, LPG, MTP, PAT) and samples from the ankle (Talus)	30	Unconfined compression Sound speed measurement DD microscopy	E_{dyn}, E c OD
	Patellar cartilage, normal and degenerated	32	Unconfined compression Sound speed measurement Histological grading Biochemistry	E_{dyn}, E c Mankin score H_2O, U, H
V	Patellar cartilage, normal and degenerated	32	Unconfined compression Ultrasound imaging Histological grading	E_{dyn}, E Qualitative Mankin score
	ACT-repaired porcine knee cartilage (Lateral facet of the femoral trochlea)	16	Mechanical indentation Ultrasound imaging Microscopic imaging	Ind. force Qualitative Qualitative
	Unpublished data			
	Patellar cartilage	8	Ultrasound indentation	E_{dyn}, R
	-	-	FE analysis with biphasic model	k

Explanation of the measurement parameters:

E_{dyn}	Dynamic modulus
E	Equilibrium Young's modulus (stress-relaxation measurement)
ν	Equilibrium Poisson's ratio (stress-relaxation measurement)
k, R	Creep rate and ultrasound reflection coefficient, respectively
c	Sound speed (determined under a preload in unconfined compression)
OD, BF	Optical density and birefringence, respectively
H_2O, U, H	Water content (H_2O), uronic acid content (U) and hydroxyproline content (H)
Ind. force	Indenter force, determined using the Artscan 200 indentation instrument

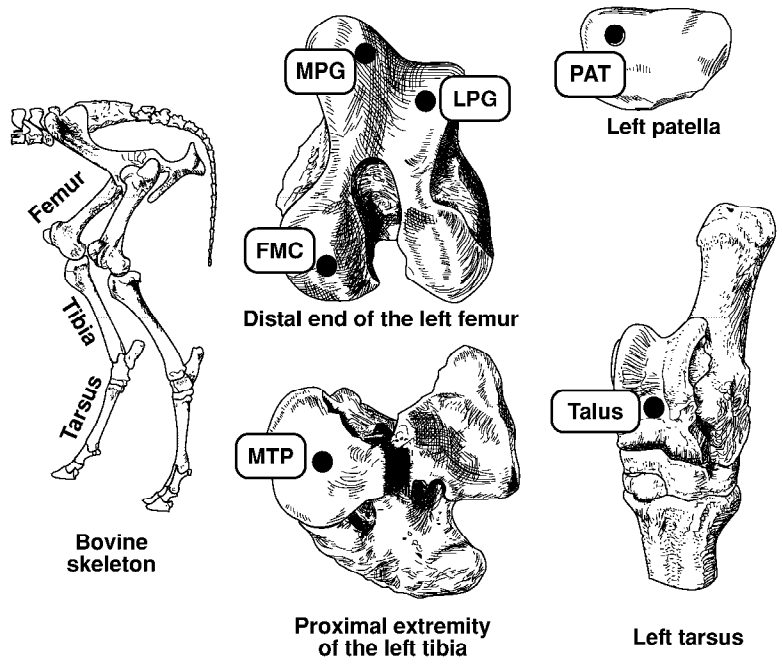

Figure 7.1: Measurement sites in the bovine knee and ankle joints.

Enzymatic digestions (I, II) of collagen, PGs or PGs with minor collagen degradation were conducted using collagenase type VII (44 h, 0.1 U/ml, Sigma Chemical Co., St. Louis, MO, USA, [151]), chondroitinase ABC (44 h, 30 U/ml, Seikagaku Co., Tokyo, Japan, [172]) or trypsin (90 min, 1 mg/ml, Sigma, [66]), respectively.

Depth-dependent variation in cartilage mechanical properties (I) was investigated by preparing a full thickness patellar sample, which was cut in depth-wise manner into ten successive slices (diameter = 2.7 mm, mean thickness = 194 $\pm$ 28 μm, as measured under a 1.7 kPa pre-stress). Each slice was tested in unconfined compression (4×5% steps, ramp speed 1 μm/s, criterium for full stress-relaxation 85 Pa/min). Subsequently, the equilibrium Poisson's ratio was determined by using the mechano-acoustic technique (prestrain 5%, strain 5%, stress-relaxation 1260 s) (Table 7.1).

Compression-tension nonlinearity of humeral articular cartilage (I) was characterized by using a cylindrical osteochondral sample (diameter = 4 mm), extracted from the peripheral part of the bovine humeral head. The sample was glued with cyanoacrylate between the smooth metallic platens of the high resolution material testing device (Figure 7.5). A stepwise stress relaxation measurement was conducted

both in compression and tension, in the direction perpendicular to the articular surface (10×0.6% steps, ramp speed 1 μm/s, criterium for full stress-relaxation 100 Pa/min) (Table 7.1).

Interrelationships between cartilage mechano-acoustic parameters and tissue composition were investigated in the patellar osteochondral specimens (II: diameter = 16 mm, $n = 17$) and full thickness cartilage disks (diameter = 4 mm, I: $n = 18$ and II: $n = 17$). In study II, the osteochondral samples were tested with the ultrasound indentation instrument, whereas the full thickness cartilage disks (I, II) were tested under unconfined compression with the mechano-acoustic material testing device (10% strain, ramp speed 2 mm/s, stress relaxation 1800 s). After the ultrasound indentation (II), sound speed (II) and unconfined compression measurements (I), the samples were divided into three groups and degraded using chondroitinase ABC, collagenase or trypsin. Ultrasound indentation, sound speed and unconfined compression measurements were conducted again after the enzymatic degradations (I and II) (Table 7.1).

Site-dependent variation of bovine articular cartilage mechanical and acoustic properties (I, III and IV) was investigated by measuring osteochondral blocks (III: $n = 18$) and full-thickness cartilage disks (diameter 3 - 4 mm, I and IV: total $n = 59$). In study III, the osteochondral blocks were harvested from three sites of bovine knee and tested with the ultrasound indentation instrument. Subsequently, full thickness cartilage samples (diameter 4 mm) were detached from the measurement sites and tested under unconfined compression (10% strain, ramp speed 2 mm/s, stress relaxation 1800-2400 s, dynamic test at 1 Hz with 1% amplitude) (Table 7.1). In studies I and IV, full thickness cartilage disks were obtained from the knee (five sites) and ankle (one site). Subsequently, the cartilage disks were tested under unconfined compression (Table 7.1). In study I, Poisson's ratios of the samples (diameter = 2.0 mm, punched from the original sample, $n = 29$) were also determined. Furthermore, in study IV ($n = 30$), the sound speed in cartilage was determined and GAG concentrations of the samples were quantified from safranin-O stained sections [94, 132] using the digital densitometry (DD) technique (Table 7.1).

Degenerated bovine knee articular cartilage samples ($n = 32$) were studied to reveal the sensitivity of ultrasound imaging and mechanical testing to detect cartilage degeneration (V). The effect of cartilage degeneration on sound speed was studied as well (IV). Initially, several fresh bovine knee joints were opened and the lateral facets of patellae were visually classified as normal or degenerated (three degenerative stages, see IV and V). Cylindrical (diameter 19 mm) osteochondral plugs were drilled from the classified sites of the patellae. Subsequently, the samples were stored in a freezer (−20 °C) for two weeks and thawed prior to analyses. According to previous studies, freezing and thawing has no or only a minor effect on the acoustic or mechanical properties of soft tissues [42, 56, 92]. The osteochondral samples were studied with the ultrasound imaging instrument (Section 7.6). Subse-

quently, cylindrical full thickness cartilage samples ($n = 32$) were prepared from the center of the osteochondral plug by using a biopsy punch (diameter 4 mm) and a razor blade. The cartilage samples were tested under unconfined compression (10% strain, ramp speed 2 mm/s, stress relaxation 2400 s, dynamic test at 1 Hz with 1% amplitude) and at the same time the sound speed was determined. The adjacent tissue surrounding the cartilage disks, was used for histological, biochemical and water content analyses.

7.3 Porcine articular cartilage samples

A total of 11 surgically treated porcine knee joints was investigated (V). The study was approved by the Animal Care and Use Committee of the University of Kuopio, Finland. Ease of availability, relatively large size of the porcine knee joint, as well as appropriate thickness of the cartilage, supported the selection of porcine as an animal model. At the age of 6 months, small pieces of cartilage were harvested from the lateral, inferior aspect of the femoral trochlea of the left knee joints. The chondrocytes were isolated and their number was multiplied in cell culture for later use. One month after cartilage biopsy, the opposite knee was operated and a cartilage lesion (diameter 6 mm, not penetrating into subchondral bone) was created on the lateral facet of the femoral trochlea ($n = 10$) and then repaired using the ACT technique. In one animal, the lesion was created, but left unrepaired. The joint from which the biopsy was taken provided a sham-operated control. After a follow-up period of three months, the pigs were sacrificed and the repair tissue, the adjacent cartilage as well as the sham operated control tissue were analyzed *in situ* with Artscan 200 indentation instrument (Artscan Oy, Helsinki, Finland). After the indentation, the same sites were analyzed with the B-mode ultrasound imaging instrument (Section 7.6). Finally, safranin-O stained sections were prepared for histological analyses.

7.4 Ultrasound indentation instrument

7.4.1 Construction and operation principle

Construction

The ultrasound indentation instrument was constructed by mounting an unfocused, 10 MHz broadband Panametrics XMS-310 contact ultrasound transducer (height 3 mm, diameter 3 mm, Panametrics Inc., Waltham, MA, USA) on the tip of a commercial arthroscopic indentation instrument (Artscan 200) [107, 108] (Figure 7.2). The ultrasound transducer was controlled with the UltraPAC-system (Physical Acoustics Corp., Princeton, NJ, USA), which comprises a 500 MHz, 8-bit linear resolution AD-board (PAC-AD-500) and a 0.5 - 100 MHz pulser-receiver board (PAC-IPR-100).

Ultrasound indentation measurement

During the ultrasound indentation measurement, an osteochondral sample was manually compressed with the ultrasound transducer. The stress applied onto the cartilage was registered with the strain gauges inside the instrument rod. The signal of the strain gauges was digitized with the AD-converter located inside the handle of the instrument. Bandpass filtering was used to enhance the signal-to-noise ratio of the ultrasound signal (II: 2.0 - 17.5 MHz, rolloff 18 dB/Oct, III: 2 - 18 MHz, rolloff 24 dB/Oct). Thickness and deformation of the sample were calculated from the ultrasound signal using the TOF principle. TOF was determined for the ultrasound signal reflected from the cartilage-bone interface (II and III) or from the elastomer-metallic platen interface (II). Finally, sample thickness and deformation were calculated by multiplying the predetermined sound speed (Section 7.7.1) with the term TOF/2. Dynamic modulus and creep rate were calculated using equations (4.4) and (4.6), respectively.

In study II, TOF was determined from the maximum value of the echoed signal. In study III, the tracking of the reflected signal was improved in the measurement program. First, Fast Hilbert transform was calculated for the signal. For function $x(t)$, the Fast Hilbert transform is determined as:

$$h_H(t) = H(x(t)) = -\frac{1}{\pi}\int_{-\infty}^{\infty}\frac{x(\tau)}{t-\tau}\,d\tau, \tag{7.1}$$

where $x(t)$ is the original windowed signal as a function of time (t) and $h_H(t)$ is the Fast Hilbert transformed signal. Subsequently, the Hilbert envelope $(E_H(t))$ was calculated for the signal as follows:

$$E_H(t) = \sqrt{x(t)^2 + h_H(t)^2}. \tag{7.2}$$

Furthermore, the signal was Hamming windowed as follows:

$$y_i = x_i[0.54 - 0.46\cos(\frac{2\pi i}{n})], \tag{7.3}$$

where y represents the output sequence, i is $0, 1, 2, ..., n-1$ and n is the number of elements in the input sequence. Finally, the TOF was calculated from the maximum value of the Hamming windowed Hilbert envelope. This method was found to be fast enough for use in real-time. It was tested with the elastomer samples of varying thickness. The method indicated correct values for elastomer thickness, in a similar manner as with the technique where TOF was determined from the maximum amplitude of the ultrasound pulse.

Ultrasound reflection measurement

During the measurement of ultrasound reflection from the articular surface, the

transducer, attached sleeve and the cartilage sample were immersed in phosphate buffered saline (PBS) and the sleeve was gently pressed against the cartilage surface (Figure 7.2). The tare-load was kept manually as small as possible. Perpendicularity between the transducer and the cartilage surface was ensured by aligning the transducer in order to obtain the maximum echo amplitude. The reflection coefficient was calculated from the equation

$$R = \frac{A_1}{A_0}, \tag{7.4}$$

where A_0 and A_1 are the maximum peak-to-peak echo amplitudes recorded from the perfect reflector (PBS-air interface, at the distance of the articular surface) and the PBS-cartilage interface, respectively.

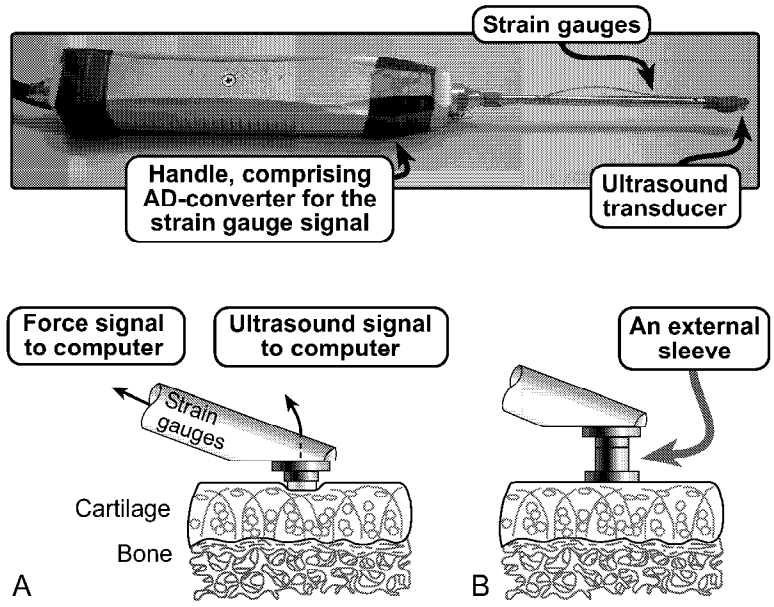

Figure 7.2: Schematic representation of the ultrasound indentation instrument and measurements. (A) During the ultrasound indentation measurement, tissue thickness and deformation were calculated from the ultrasound signal while the stress induced onto the tissue was detected with the strain gauges inside the instrument rod. (B) During the ultrasound reflection measurement, an external sleeve was used to maintain the transducer at a constant distance from the articular surface.

7.4.2 Software

Software for the data acquisition and analysis was developed in the LabVIEW G-language environment (version 6i, National Instruments, Austin, TX, USA) [73] (Figure 7.3). The software was divided into independent sections for ultrasound indentation and ultrasound reflection measurements as well as for data-analysis. The quality of the measurements may be monitored continuously. The current strain or stress and the predefined limits of acceptance are shown for the user as a progress bar. The bar guides the user during the measurement. The measurement site can be located onto an image of the articular surfaces of the knee joint, enabling the creation of a database containing information on the cartilage properties at different sites.

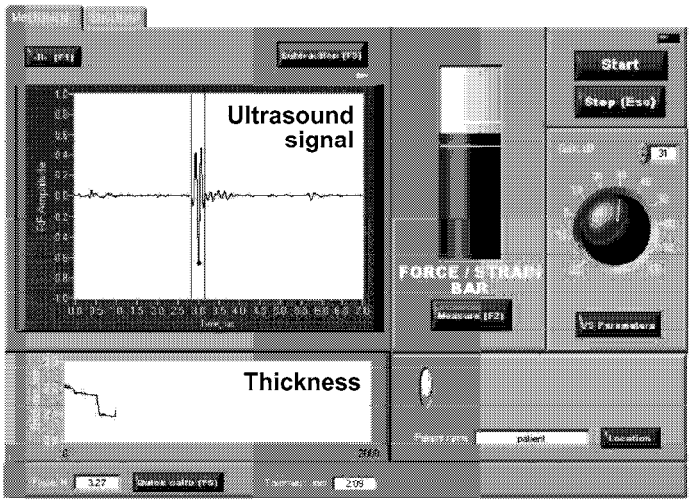

Figure 7.3: Screen capture of the ultrasound indentation software demonstrating how the ultrasound signal, thickness analysis and the force control are viewed by the user during the ultrasound indentation measurement.

7.4.3 Ultrasound indentation and reflection measurements

Ultrasound indentation measurements

The dynamic moduli of the elastomers were measured by inducing several consecutive instantaneous compressions on the sample (prestress 140 kPa, stress 600 - 700 kPa) (II). The average of the four largest moduli values (equation 4.4) was chosen to represent the elastomer dynamic modulus. The measurement was repeated several times and the final outcome was obtained as a mean value.

In study II, (after a brief 140 kPa prestress) 1 MPa constant stress was instantaneously applied onto the cartilage and maintained for 20 s. The dynamic modulus was determined instantaneously after the 1 MPa stress level was reached and the creep rate (equation 4.6) was determined from the first 10 s after inducing the 1 MPa stress. The dynamic modulus and creep rate were obtained as mean values from the measurements showing the three largest moduli values.

In study III, several instantaneous compressions were applied onto cartilage (215 kPa prestress (duration 3 s), followed by compressive strain of 4%). The dynamic modulus was determined instantaneously after the 4% strain was reached. The mean value of three largest moduli was chosen to represent the cartilage dynamic modulus.

Ultrasound reflection measurements
In the ultrasound reflection measurements (II, III), the maximum ultrasound echo amplitude from the PBS-cartilage interface was measured several times per sample and averaged.

7.5 Numerical simulations

7.5.1 Effect of the varying sound speed on ultrasound indentation

The error induced by the variable sound speed on ultrasound indentation was simulated by modeling cartilage to be an isotropic and instantaneously incompressible (Poisson's ratio = 0.5) elastic material [69, 111]. The indenter diameter of 3 mm was used in all simulations. In the first simulation, the sound speed was varied around 1630 m/s (predefined sound speed) and the error induced on the dynamic modulus was calculated for cartilage of different thicknesses. Simulations were carried out for the tissue thicknesses of 300 - 5250 μm to cover typical thickness of thin (bovine) and thick (human) cartilage [12, 14]. In addition, the error induced on the determined thickness and dynamic modulus of cartilage were calculated for the cases where the mean sound speed of the whole material or each test site or joint (knee or ankle), instead of the true sound speed, was used.

7.5.2 Finite element modeling

FE analysis of ultrasound indentation creep measurements was investigated using the poroelastic cartilage model (equivalent to biphasic model) [119, 158] which was coded in a commercial FE package (Abaqus v.5.8, Hibbitt, Karlsson & Sorensen Inc., Pawtucket, RI, USA). An axisymmetric FE model cartilage consisted of eight-node poroelastic elements (CAX8P). Typical values of mechanical parameters for human cartilage were used [116, 119]: compressive Young's modulus of 0.79 MPa, Poisson's ratio of 0.02, permeability of 4.7×10^{-15} m^4/Ns and porosity of 78%. Mesh of the model and loading pressure (84.4 kPa) were similar to those in the study by

Suh and Spilker (1994) [158]. Nonlinearity of the geometry was utilized. In the FE analysis, the rigid, impervious, plane-ended indenter (*i.e.* ultrasound transducer) was compressed against the cartilage (ramp duration 1 second, obtained from experimental measurements) after which the force was held constant until the mechanical equilibrium was obtained (4500 seconds). The creep rate of the first 20 seconds was analyzed as in the experimental tests for the thickness values of 1 mm, 1.5 mm, 2 mm, 3 mm, 4 mm and 5 mm. The effects of variations in the values of Young's modulus, Poisson's ratio and permeability on the creep rate were studied with thickness values of 1 mm, 3 mm and 5 mm.

7.6 Ultrasound imaging

Ultrasound imaging instrument (Dermascan-C, 20 MHz, Cortex Ltd., Hadsund, Denmark, Figure 7.4) was used for the characterization of normal or degenerated bovine ($n = 32$) and ACT-repaired porcine ($n = 11$) cartilage samples (V). During the measurements, the samples were immersed in PBS containing enzyme inhibitors. The Dermascan-C instrument consists of a portable computer and a handheld measurement probe. The B-mode image is produced by mechanical scanning with a focused 20 MHz ultrasound transducer.

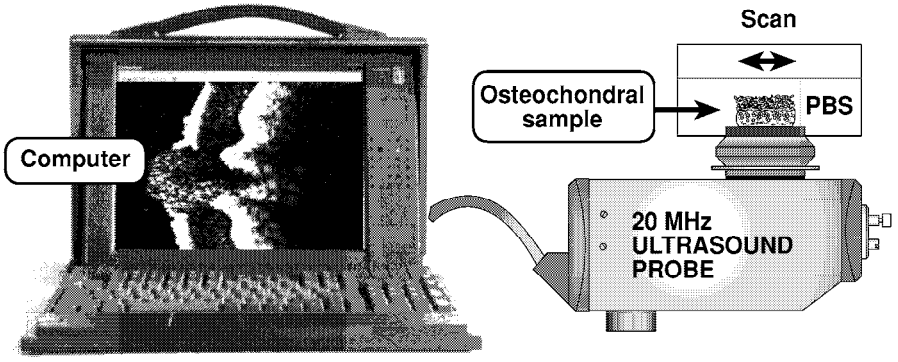

Figure 7.4: B-mode ultrasound imaging instrument (Dermascan C, Cortex Ltd., Denmark). During measurements, articular cartilage samples were placed into a custom-made sample holder.

7.7 Reference methods

7.7.1 Mechano-acoustic measurements

As a reference, and to compare with the results obtained using the ultrasound-indentation instrument, the thickness, the sound speed, the Young's modulus at equilibrium and dynamic modulus (or instantaneous modulus) of the cartilage samples were determined in unconfined compression geometry. Measurements were carried out using a custom-made computer-controlled high resolution mechano-acoustic material testing device (I - V) (Figure 7.5). The device consisted of a Newport PMA500-C (Newport Corp., Irvine, CA, USA) controller, Newport PMA 10347 actuator and a Sensotec 31/1430-04 (Sensotec, Inc., Columbus, OH, USA) force transducer (max. load 10 kg). The force signal was controlled using an RDP E308 (RDP Electronics Ltd., Wolverhampton, UK) transducer indicator and digitized using National Instruments NI 6023E, 200 kS/s, 12-bit resolution DAQ card. The resolution of the device was 0.1 μm and 5 mN for position and load, respectively. Further, sampling rates were 50 Hz, 200 Hz and 500 MHz for position, load and ultrasound signal, respectively. A Panametrics VM-116, contact ultrasound transducer (center frequency 10.3 MHz, 7.1 - 14.2 MHz (-3 dB)) acted as the upper compressive platen during the acoustic measurements. The ultrasound signal was controlled with the UltraPAC-system. A bandpass filter (6.0 - 12.5 MHz, rolloff 18 dB/Oct) was used to enhance the ultrasound signal-to-noise ratio. Software for the data acquisition and analysis was developed with LabVIEW. Bovine synovial fluid was used for minimizing friction between the cartilage sample and compressive platens during the measurements.

The sound speed in the cartilage was determined after equilibrium preloading using the pulse-echo technique. The TOF was determined as the travel time of the maximum amplitude of the ultrasound pulse back and forth through the sample, while the cartilage thickness at preload was determined as the distance between the compressive platens. The TOF measurement was verified by measuring the correct sound speed value in distilled water at any ultrasound transducer-metallic platen distance. All measurements were conducted at room temperature (20 °C).

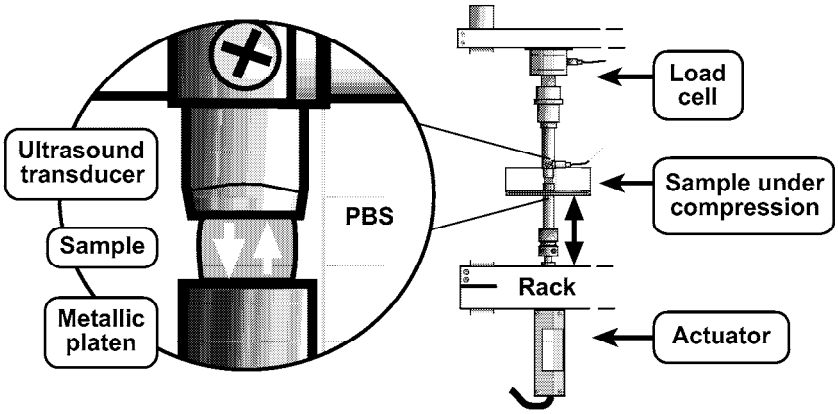

Figure 7.5: Mechano-acoustic, high-resolution material testing device. All mechanical reference measurements were conducted in unconfined compression geometry. Sound speed of the elastomers and cartilage samples were determined using the 20 MHz ultrasound transducer, which acted as the upper metallic platen during the measurements.

Poisson's ratios of the samples were determined under unconfined compression with custom made mechano-optical device [82] (see I: Figure 2). The device consisted of a custom made sample chamber, Polaroid DMC 1 CCD-camera (Polaroid Corp., Waltham, MA, USA) and Olympus BH-2 light microscope (Olympus Optical Co. Ltd., Shinjuku-ku, Tokyo, Japan). The compression was induced by a micrometer and the mean lateral dilatation of the sample was determined optically. The resolution of the device was 1.9 μm and 1.0 μm in lateral and axial directions, respectively. Data analysis was conducted with the IP-Lab program (version 3.2.4, Scananalytics Inc., Fairfax, VA, USA). Bovine synovival fluid was used for lubrication of contact surfaces to minimize friction.

7.7.2 Microscopical, histological and biochemical analyses

The GAG content of the samples was analyzed with the DD technique [94, 132] as the mean optical density (OD) of five safranin-O stained full-thickness cartilage sections per cartilage sample (III and IV). Determination of OD is based on the general Beer-Lambert law, defined as $\mathcal{A}(\lambda) = a_c(\lambda)bC$, where $\mathcal{A}$ is the measured absorbance (=OD), $a_c(\lambda)$ is wavelength (λ) dependent absorptivity coefficient, b is the path length of the light and C is the concentration. During the measurements transmittance ($\mathcal{T}(\lambda)$) of the light was determined. Transmittance is defined as $\mathcal{T}(\lambda) = I(\lambda)/I_0(\lambda)$, where $I(\lambda)$ is the intensity of light after it passes through the sample

and $I_0(\lambda)$ is the initial intensity. The relation between $\mathcal{A}(\lambda)$ and $\mathcal{T}(\lambda)$ is as follows

$$\mathcal{A}(\lambda) = -\log_{10}(\mathcal{T}(\lambda)) = -\log_{10}(\frac{I(\lambda)}{I_0(\lambda)}). \tag{7.5}$$

The device consisted of a Leitz Orthoplan microscope (Leitz Messtechnik GmbH, Wetzlar, Germany) and a Peltier-cooled 12-bit Photometrics CH-250-A CCD-camera (Roper Scientific Inc., Tucson, AZ, USA). Data analysis was conducted with the IP-Lab program (version 3.5.5).

Cartilage degeneration was graded histologically using the Mankin's scoring method [112] (IV and V). In Mankin's scoring, the different stages of tissue degeneration are identified by evaluating the cartilage structure, cell alterations, safranin-O staining (*i.e.* GAG concentration) and tidemark integrity (IV: Table 1). The scoring of the blind-coded samples was independently conducted by three researchers. The final Mankin's score was calculated as a mean of the three evaluations.

In study IV, wet weight of the bovine cartilage samples was measured. Subsequently, the samples were freeze-dried, the dry weight of cartilage tissue was determined and tissue water content was calculated from this information. The PG content of the samples was estimated by quantifying the total uronic acid content biochemically [21]. The collagen content of the samples was estimated by spectrophotometric assay of hydroxyproline after hydrolysis of the tissue [149]. The biochemical procedures are presented in more detail in study IV.

7.8 Statistical analyses

Non-parametric Wilcoxon's signed ranks test was used for analyzing the statistical significance of differences between the cartilage parameters before and after enzymatic degradation (I and II) and for comparing the stiffness of the normal and ACT-repaired porcine cartilage (V). Nonparametric Kruskall-Wallis H test was used for testing the site-dependent variation of the measured parameters (I, III and IV). Kruskall-Wallis Post Hoc test [152] was used for comparing differences in parameters between the measurement sites (III).

Pearson's correlation coefficient (r) was used to indicate the strength of linear association between two numerical variables. Spearman's correlation coefficient ($r_{Spearman}$) was used for expressing the strength of the association between a non-continuous variable (Mankin's score [112], IV and V), and other variables. SPSS statistical software (SPSS Inc., version 8.0, Chicago, IL, USA) was used for statistical comparisons.

Commonly, the reproducibility of the repetitive measurements of a sample is defined in terms of a coefficient of variation (CV). CV is calculated as a ratio of standard deviation (σ_x) and mean ($\bar{x}$) of the repeated measurements of the parameter x. For several samples, the CV is a root mean square averaged value ($\mathrm{CV_{RMS}}$)

[20]. In ultrasound indentation, the reproducibility of the elastomer thickness and dynamic modulus measurements (II) was determined by using the CV_{RMS}. The reproducibility of the thickness, dynamic modulus, ultrasound reflection coefficient (III) and creep rate measurements of articular cartilage was determined in terms of a standardized coefficient of variation (sCV) [20, 129]. sCV takes into account the biological variation of the measured parameters and it is calculated as follows:

$$\mathrm{sCV} = \frac{\sqrt{\left(\sum_{i=1}^{n}(\sigma_{x_i}/\overline{x}_i)^2\right)/n}}{4\sigma_\mu/\overline{\mu}} = \frac{\mathrm{CV_{RMS}}}{4\sigma_\mu/\overline{\mu}}, \tag{7.6}$$

where σ_μ and $\bar{\mu}$ are the standard deviation and average of the parameter within the population, respectively. A standardized coefficient of variation gives a better indication of the true diagnostic sensitivity of the measurements than the conventional short-term precision obtained with the CV [20, 129]. The smaller the sCV (or CV_{RMS}) value, the better the reproducibility (0% indicates a perfect reproducibility).

Interoperator reliability of the ultrasound indentation parameters (thickness, dynamic modulus and ultrasound reflection coefficient) was determined by using the intraclass correlation coefficient (1 indicates perfect reliability). The interoperator reliability test was conducted by three investigators (patellar cartilage, $n = 8$, measurement protocol was the same as in study III).

Chapter VIII

Results

8.1 Site-dependent variation of mechano-acoustic properties

Significant site-dependent variation ($p < 0.05$, Kruskall-Wallis H test) was revealed in the thickness, dynamic modulus, equilibrium Young's modulus, Poisson's ratio, sound speed and GAG concentration (OD) of the bovine knee joint cartilage (Figure 8.1). In the knee joint, cartilage thickness varied from 800 μm to 1880 μm. The lowest moduli values were recorded in MTP (E_{dyn} = 1.96 ± 1.19 MPa, E = 0.17 ± 0.10 MPa) and the highest in the LPG (E_{dyn} = 10.61 ± 4.59 MPa, E = 0.53 ± 0.15 MPa). In the ankle, cartilage stiffness was high (E_{dyn} = 12.88 ± 3.57 MPa, E = 0.62 ± 0.22 MPa) and the tissue was relatively thin (435 ± 53 μm). Equilibrium Poisson's ratio was the highest in the MTP (0.39 ± 0.07) and lowest in the LPG (0.19 ± 0.04).

Sound speed varied from 1531 m/s to 1683 m/s in the knee and was highest in the ankle (1721 ± 26 m/s). OD of the safranin-O stained sections varied in the range of 0.19 - 0.83 in the knee and was 1.29 (± 0.05) in the ankle.

8.2 Ultrasound indentation

8.2.1 Elastomers

The thickness values obtained with the novel instrument correlated linearly with the elastomer true thickness (r = 1.000, n = 8, $p < 0.01$, mean error 3.2% ± 1.5%, II: Figure 2A). Dynamic moduli, as obtained with the novel instrument, were found to correlate linearly with the elastomer reference dynamic moduli (r = 0.994, n = 13, $p < 0.01$, Figure 8.2A). For elastomers (n = 21), the reproducibilities in thickness and stiffness measurements (CV_{RMS}) were 1.8% and 8.2%, respectively.

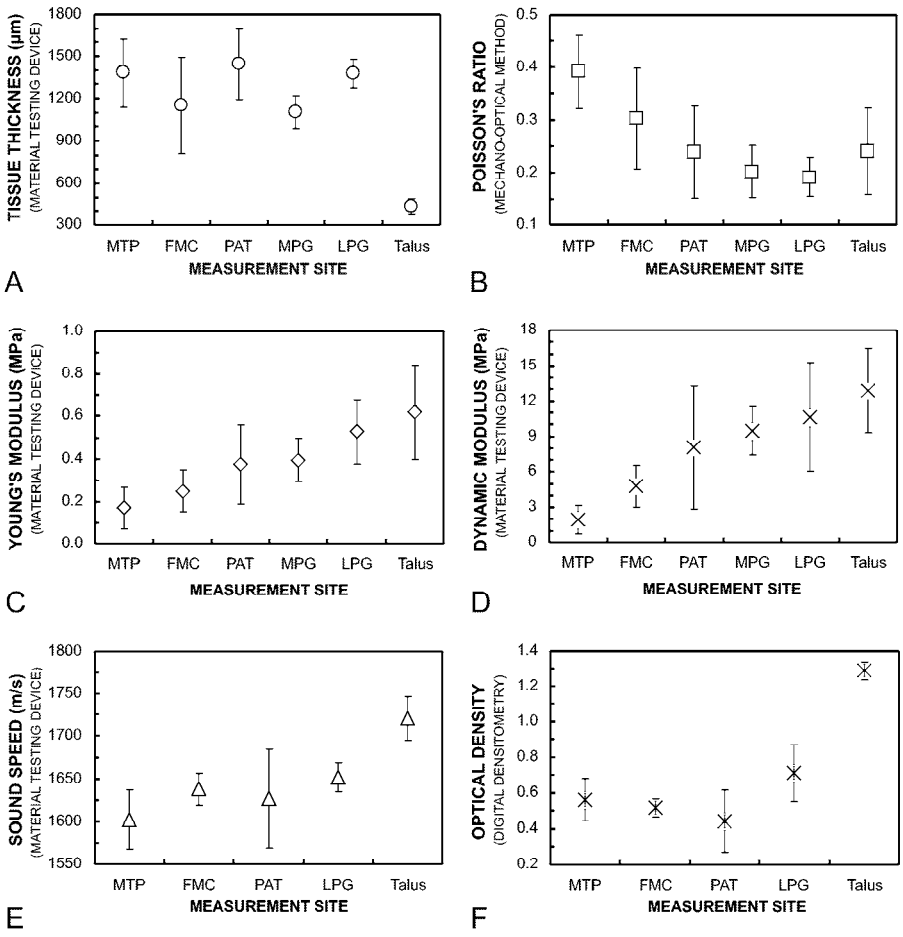

Figure 8.1: Site-dependent variation of the thickness, Poisson's ratio, equilibrium and dynamic modulus (1 Hz), sound speed and optical density, *i.e.* glycosaminoglycan content, in the bovine knee articular cartilage (mean ± SD).

8.2.2 Normal cartilage

The dynamic modulus of the visually normal bovine knee articular cartilage, as obtained with the ultrasound indentation instrument, correlated linearly ($r = 0.913$, $p < 0.01$) with the reference values (Figure 8.2B). Values of dynamic modulus and ultrasound reflection coefficient of the articular surface were site-dependent ($p <$

0.05, Kruskall-Wallis H test). The dynamic modulus was significantly ($p < 0.05$, Kruskall-Wallis Post Hoc test) higher at LPG (10.14 ± 3.11 MPa) than at MTP (2.92 ± 1.38 MPa). In FMC, the dynamic modulus was 4.63 ± 1.32 MPa (Figure 8.2C). Ultrasound reflection coefficient from the articular surface was significantly ($p < 0.05$) smaller at MTP (2.04 ± 0.73%) than at other sites (FMC: 4.22 ± 0.88%, LPG: 4.43 ± 0.83%) (Figure 8.2C). GAG content (OD) of cartilage, which was found to be site-dependent ($p < 0.05$), correlated linearly with the tissue dynamic modulus ($r = 0.678$, $p < 0.01$) and with the equilibrium Young's modulus (reference device, $r = 0.874$, $p < 0.01$) (III: Figure 3B), but was not significantly related to the ultrasound reflection coefficient ($r = 0.294$, $p = 0.24$).

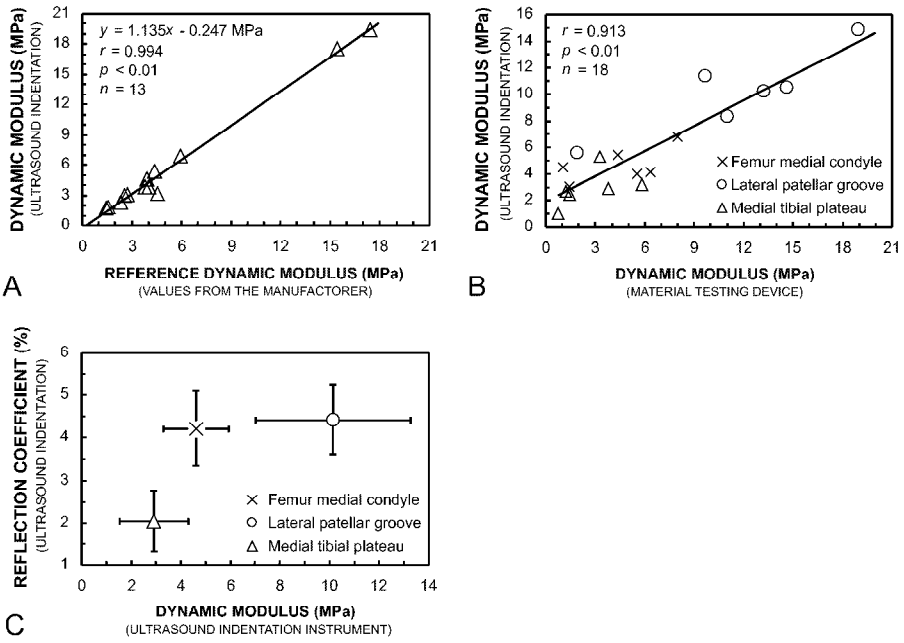

Figure 8.2: Dynamic modulus of (A) elastomers and (B) cartilage, as determined with the ultrasound indentation instrument, correlated linearly with the reference dynamic moduli. (C) Cartilage dynamic modulus, as determined with the ultrasound indentation instrument (mean ± SD, $n = 6$ per site), was significantly (Kruskall-Wallis Post Hoc test) higher in the lateral patellar groove than in the medial tibial plateau. Ultrasound reflection coefficient was significantly lower at medial tibial plateau than at other sites. Combined results from the indentation and the reflection measurements could be used to differentiate cartilage properties between the test sites.

For normal cartilage, reproducibility (sCV) was 3.0%, 5.2%, 1.7% and 4.0% in thickness, dynamic modulus, ultrasound reflection coefficient and creep rate measurements, respectively (FMC, LPG, MTP, $n = 6$ per site).

Interoperator reliability (intraclass correlation coefficient) was 0.905, 0.669 and 0.786 in thickness, dynamic modulus and ultrasound reflection coefficient measurements, respectively (patellar cartilage, $n = 8$). The measurements were conducted at the center point of the sample by three investigators.

To establish a representative reference population for calculating single user sCV (see denominator in equation 7.6), the data from this thesis work ($n = 26$) and our recent study [144] ($n = 30$) was combined (same user in all tests). In the interoperator reliability test ($n = 8$), single user sCV was 0.5%, 4.3% and 0.4% for thickness, dynamic modulus and ultrasound reflection coefficient measurements, respectively.

8.2.3 Enzymatically degraded cartilage

The specific structural and functional changes, as induced by enzymatic digestions, could be specifically detected with the ultrasound indentation technique (II: Table 1). Enzymatic degradation using trypsin or collagenase induced -31% ($p < 0.05$) or -23% ($p = 0.08$) decrease in the dynamic modulus, respectively (II: Table 1). The creep rate of the patellar cartilage increased with respect to the magnitude of PG cleavage, +118% ($p < 0.05$) after trypsin and +25% ($p = 0.17$) after chondroitinase ABC degradation (Figure 8.3A). Specific collagen degradation with collagenase decreased more extensively the ultrasound reflection coefficient (-54%, $p < 0.05$) (Figure 8.3B) than degradation with trypsin (-17%, $p = 0.08$) (Figure 8.3C). PG cleavage with chondroitinase ABC induced no changes in the ultrasound reflection from cartilage surface (Figure 8.3D). However, the penetration front of PG cleavage after chondroitinase or trypsin could be detected with the ultrasound technique (Figure 8.3C, D).

In study I, it was shown that the PGs affect primarily the static properties of cartilage, while collagens are mainly responsible for its dynamic stiffness. On the other hand, ultrasound reflection from the cartilage surface was the most sensitive parameter for the detection of cartilage collagen degradation (II). Thus, in ultrasound indentation, combined creep and ultrasound reflection results (Figure 8.4) distinguished PG loss and superficial collagen degradation specifically.

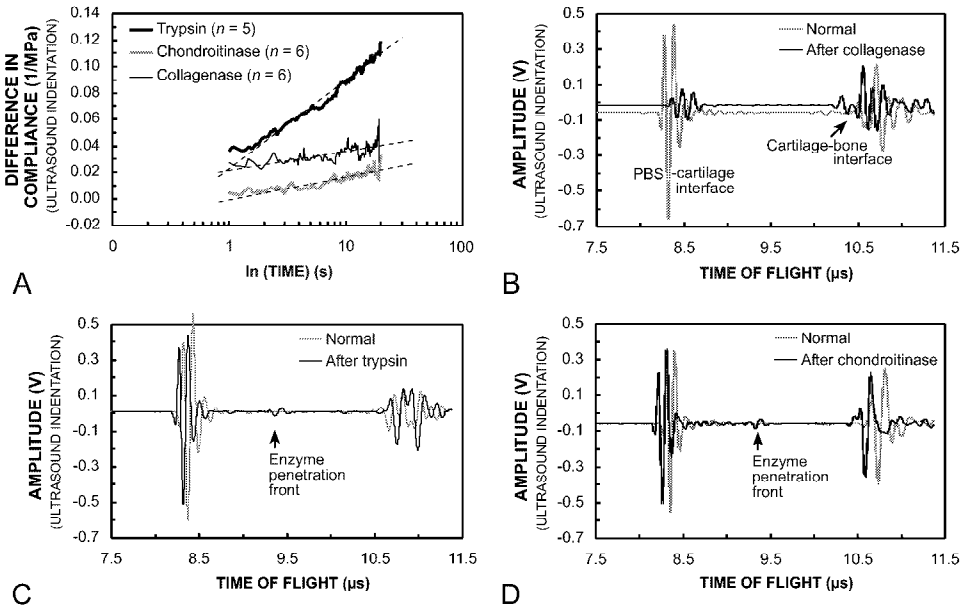

Figure 8.3: (A) The mean change in the creep rate (*i.e.* slope for the logarithmic time vs. compliance (strain/stress) ratio) after trypsin, chondroitinase ABC and collagenase treatments. The creep rate increased with respect to the magnitude of proteoglycan cleavage. Typical A-mode ultrasound signals registered before and after (B) collagenase, (C) trypsin and (D) chondroitinase ABC degradation. Collagenase (collagen type II degradation) reduced ultrasound reflection from the articular surface more than trypsin. Pure proteoglycan cleavage by chondroitinase ABC induced no significant changes in the ultrasound reflection coefficient. The penetration front of proteoglycan cleavage after trypsin or chondroitinase ABC could be detected with the ultrasound measurement (C).

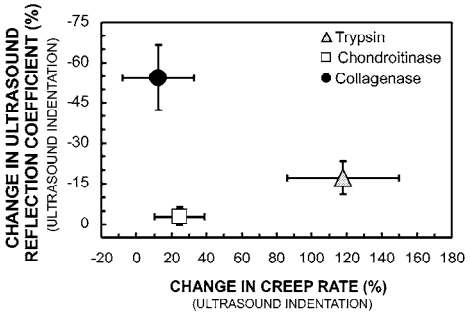

Figure 8.4: The change in the ultrasound reflection coefficient from the PBS-cartilage interface as a function of the change in creep rate (slope of the logarithmic time vs. compliance plot) after trypsin ($n = 5$), chondroitinase ABC ($n = 6$) or collagenase ($n = 6$) treatments (group mean $\pm$ SEM). In enzymatically degraded cartilage, combined measurement of creep rate and ultrasound reflection distinguished superficial collagen fibril network damage from proteoglycan depletion.

8.2.4 Effect of the varying sound speed on ultrasound indentation

Sound speed in cartilage remained nearly constant during enzymatic treatments (Table 8.1). The only significant decrease in the sound speed was detected in the trypsin group (-1.2% $\pm$ 1.1%). After the enzymatic degradations (II), the maximum single decrease (-3.6%) was detected in a collagenase digested sample. In ultrasound indentation, this would induce errors of +3.7% and +0.04% on the thickness and dynamic modulus, respectively (calculated using a mean thickness of 1731 μm for all enzymatically degraded samples).

Simulation of the error (IV) revealed that the use of a mean sound speed in knee joint or talus cartilage, instead of the true speed, induced a maximum mean error of 2.9 $\pm$ 3.8% (mean $\pm$ 2SD) on thickness (patella) and 0.9 $\pm$ 1.3% on dynamic modulus (talus) (IV: Table 2). Instead of using the mean sound speed in the tested samples (1627 m/s), the use of the maximum registered sound speed (1754.2 m/s, talus sample, thickness 395 μm) generated a correction of +7.8% and +6.2% on the thickness and dynamic modulus of talus cartilage, respectively. Furthermore, the correction with the minimum registered speed (1531.7 m/s, patella sample, thickness 1410 μm) was -5.9% and -0.9% for the thickness and dynamic modulus values of patellar cartilage, respectively.

The simulations revealed that the errors were very similar when the mean sound speed values in the specific measurement site, joint or whole material were utilized as predefined values (IV: Table 2). Simulated errors in the dynamic moduli were

smaller in thick cartilage (thickness: 2 - 4 mm, typical to human knee cartilage) than in thin cartilage (thickness: 0.4 - 2 mm, typical to bovine knee or ankle cartilage) (Figure 8.5).

Table 8.1: Sound speed (mean ± SD) (m/s) in bovine patellar cartilage before and after enzymatic degradation with trypsin, chondroitinase ABC or collagenase.

Enzyme	Before degradation	After degradation	Change (%)
Trypsin (1 mg/ml, 90 min, $n = 5$)	1614 ± 22	1595 ± 14	-1.2 ± 1.1[a]
Chondroitinase ABC (0.1 U/ml, 44 h, $n = 6$)	1605 ± 10	1605 ± 18	+0.0 ± 0.8
Collagenase type VII (30 U/ml, 44 h, $n = 6$)	1606 ± 31	1580 ± 23	-1.6 ± 1.6

[a] $p < 0.05$, Wilcoxon's signed ranks test.

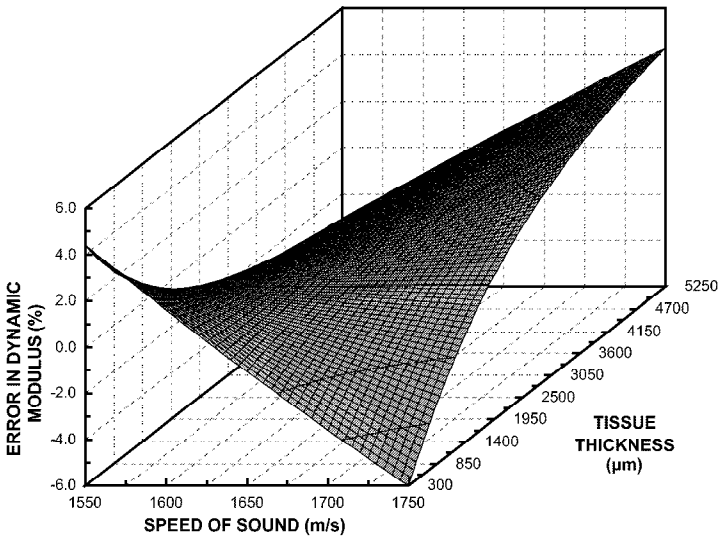

Figure 8.5: The simulated error in the dynamic modulus determined with the ultrasound indentation instrument and by assuming a constant sound speed (1630 m/s). In the simulation, cartilage was modeled as an isotropic, incompressible (Poisson's ratio = 0.5) elastic material [69, 111]. In the simulation, an indenter diameter of 3 mm was used and the sound speed varied around 1630 m/s (predefined sound speed).

8.2.5 Finite element analysis

FE analysis revealed that tissue thickness modifies significantly the creep compliance of cartilage (Figure 8.6). It is noteworthily that in thin cartilage (1 mm), the short-term compliance differed significantly from that found in thicker (> 1.5 mm) cartilage. During the first 20 seconds of indentation, the creep rate decreased as the cartilage thickness increased (Figure 8.6B). In the FE-model, a decrease of the Young's modulus of the cartilage solid matrix (1.2 MPa → 0.4 MPa) increased the creep rate by 36%, 63% and 64% for cartilage of 1 mm, 3 mm and 5 mm in thickness, respectively. An increase in the cartilage permeability (2.3×10^{-15} m^4/Ns → 7.1×10^{-15} m^4/Ns) elevated the creep rate by 105%, 78% and 77% for cartilage with 1 mm, 3 mm and 5 mm thickness, respectively. Increase of Poisson's ratio of the solid matrix (0.02 → 0.2) induced a decrease of less than 9% in the creep rate with all values of cartilage thickness.

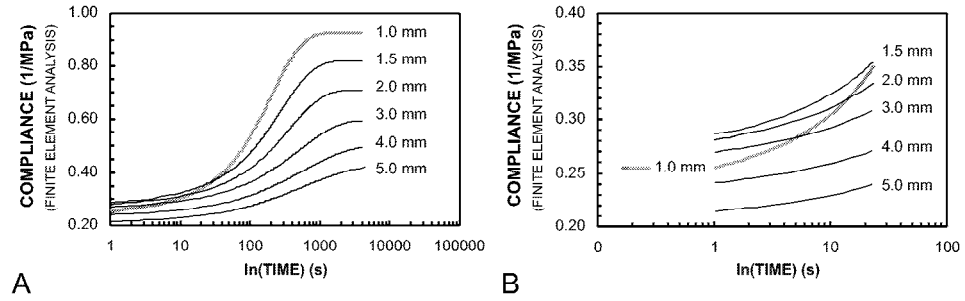

Figure 8.6: Finite element analysis of the creep compliance of biphasic cartilage for (A) equilibrium and (B) for the first 20 seconds. Tissue thickness modified significantly the creep compliance (or creep rate) of cartilage. In thick (3 - 5 mm) cartilage, such as in human cartilage, changes in biphasic material parameters control strongly the creep rate and the creep rate is less dependent on tissue thickness.

8.3 Combined ultrasound imaging and mechanical measurements

8.3.1 Degenerated bovine knee cartilage

Dynamic modulus of the bovine cartilage samples correlated negatively with the Mankin's score ($r_{Spearman}$ = -0.793, n = 32, $p < 0.01$, Figure 8.7A). All visually degenerated samples (mean Mankin's score = 4) and five visually intact cartilage

samples (mean Mankin's score = 1) were softer (dynamic modulus < 2.1 MPa) than the histologically normal samples (dynamic modulus 13.8 ± 3.2 MPa, Mankin's score = 0) (Figure 8.7A). The equilibrium Young's modulus of the normal and degenerated samples varied between 0.01 MPa - 0.55 MPa and correlated negatively with the Mankin's score ($r_{Spearman}$ = -0.699, $n = 32$, $p < 0.01$, Figure 8.7B).

Cartilage degeneration could be visualized by ultrasound imaging (Figure 8.8). Visually normal cartilage surface showed a continual, smooth and strong echoband (Figure 8.8A, B), while the degenerated samples showed a roughened and weak echoband (Figure 8.8C, D, V: Figure 3).

8.3.2 Engineered porcine cartilage

B-mode ultrasonic imaging offered detailed information on the structure of cartilage and subchondral bone in control, unrepaired and repaired porcine tissue (Figure 8.9). Ultrasonic images revealed the highly echogenic internal structure of porcine cartilage. Both histological sections and ultrasound images of unrepaired or repaired tissue revealed the extent and area of the lesion. In the unrepaired site, the lesion was not spontaneously filled by the new tissue to the level of the adjacent cartilage. In the repaired site, the defect was better filled, although the articular surface appeared to be either concave or convex. In the repaired and unrepaired sites, the erosion of the subchondral bone and distinct abnormalities in the internal tissue structure could be sensitively detected from the ultrasonic and histological images. Histological, ultrasonic and mechanical analyses revealed that after three months of follow-up, the quality of the repair tissue was not at the level of normal cartilage and that the focal subchondral erosion was relatively strong.

Cartilage stiffness, as indicated by the indenter force measured with the mechanical indentation instrument (Artscan 200), was significantly ($p < 0.05$, Wilcoxon's signed ranks test) lower in the repaired tissue (0.6 ± 0.3 N, $n = 6$) than in the adjacent cartilage (1.6 ± 0.1 N, $n = 7$) or in the sham operated contralateral site (1.9 ± 0.4 N, $n = 7$).

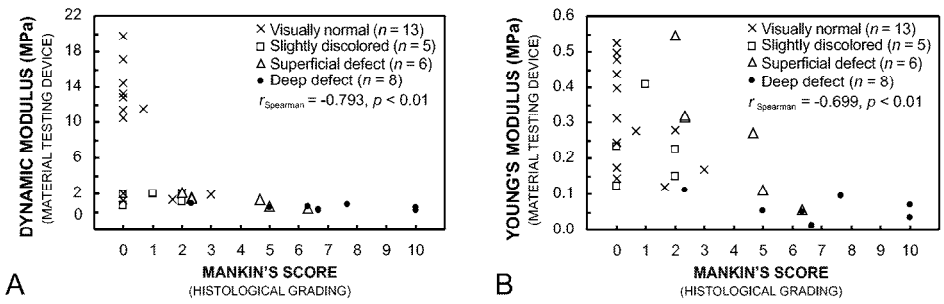

Figure 8.7: (A) Dynamic modulus of the normal and degenerated bovine articular cartilage samples correlated negatively with the cartilage Mankin's score. Five visually intact cartilage samples showed a decreased dynamic modulus, revealing that the visual assessment was insensitive and that the mechanical properties of visually intact cartilage may indeed have deteriorated. (B) The equilibrium Young's modulus of cartilage correlated negatively with the Mankin's score although it was not as sensitive as the dynamic modulus in detecting the early degenerative changes.

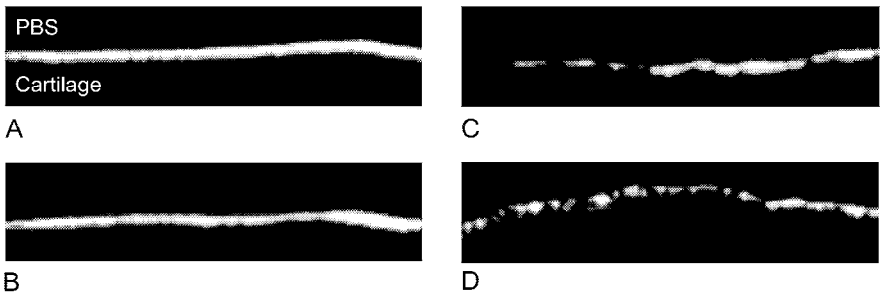

Figure 8.8: Representative ultrasound images of the visually (A, B) normal or (C, D) degenerated bovine patellar cartilage. Cartilage surface roughening (C, D), evident in ultrasound images, was not visually detectable. Mankin's scores of the representative samples were 0 (A, B), 1 (C) and 2 (D).

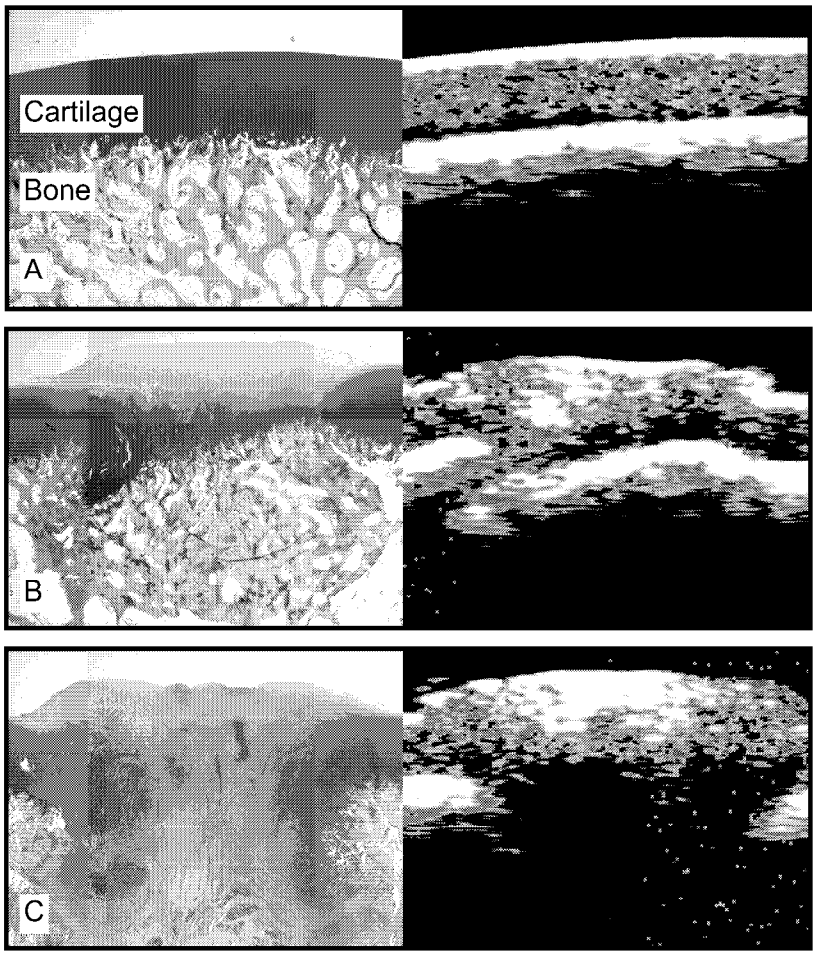

Figure 8.9: Safranin-O stained microscopic sections (left) and the corresponding B-mode ultrasound images (right) from the (A) contralateral normal cartilage and (B and C) tissue repaired using autologous chondrocyte transplantation. Ultrasonic imaging reveals the highly echogenic internal structure of porcine cartilage and detects the extent and area of the lesions. Both histological and ultrasonic analyses revealed abnormalities in the internal tissue structure. In conjunction with the changes in repair tissue, severe subchondral erosion is detected underneath the repair site. Size of the ultrasonic and histological images is $\sim$ 1.2 cm $\times$ 0.9 cm (width $\times$ height).

Chapter IX
Discussion

In this thesis, mechanical and acoustic methods were developed and tested to improve the quantitative evaluation of articular cartilage quality. Initially, cartilage structure function relationships were investigated in order to understand interrelationships between certain tissue components and mechanical properties. A prototype of an arthroscopic ultrasound indentation instrument was designed, constructed and validated by using experimental tests and numerical simulations. Furthermore, B-mode ultrasound imaging and quantitative mechanical measurements were used to diagnose cartilage degeneration and to monitor tissue healing after ACT surgery.

A significant site- and depth-dependent variation was revealed in the cartilage mechanical properties (I). Experimental measurements in compression and tension indicated nonlinear compression-tension behavior of articular cartilage in the direction perpendicular to articular surface. With the fibril-reinforced poroelastic biphasic FE model, this behavior was successfully described. Enzymes were used for degrading cartilage collagen and PGs selectively. It was found that collagen degradation, as induced by collagenase, affects mainly the dynamic stiffness but has an effect on the equilibrium properties as well. The decrease of the cartilage equilibrium modulus, as induced by collagenase, might be explained partly by the secondary PG loss [141] that was detected using the digital densitometry. A major decrease of the cartilage PG content, as induced by trypsin, reduced the tissue equilibrium modulus significantly. These results aided the development of the instrumentation ultimately designed for the clinical evaluation of cartilage status. First, the collagen disruption could be detected by measuring dynamic (or instantaneous) response of the tissue. Second, if the dynamic response is normal (*i.e.* collagen fibrils are intact), a longer-term measurement may be conducted for the detection of PG depletion. Recent FE analysis with the fibril reinforced poroelastic model were consistent with experimental findings of the study I [96].

In study II, the prototype of an arthroscopic instrument, integrating ultrasound and indentation measurements, was constructed and experimentally validated. With

the prototype, dynamic modulus, creep rate and ultrasound reflection from the articular surface were determined before and after enzymatic degradation of cartilage PGs or collagen. The creep rate, as determined in a 20 s creep measurement, was found to be a sensitive parameter for detecting cartilage PG degradation. Ultrasound reflection from the cartilage surface was the most sensitive parameter at detecting this superficial collagen damage. The measurements of ultrasound reflection and tissue creep rate permitted us to measure normal cartilage, collagen damage or PG depletion both sensitively and specifically.

The biphasic (poroelastic) [119] FE model revealed that during the first 20 seconds of indentation, the creep rate was sensitive to biphasic material parameters and decreased as cartilage the thickness increased, *i.e.* thickness modified significantly tissue creep compliance. However, in thick cartilage ($\geq$3 mm), changes in the biphasic material parameters govern the creep whereas the thickness has a only a minor effect. In study II, the cartilage thickness remained constant during enzymatic treatments and, therefore, differences in the creep-rate reflected true variations in the material properties. Before one can fully interpret the results of creep measurement, and to avoid possible uncertainties related to the measurement protocol and to effects by the variable tissue thickness, a more detailed theoretical approach will need to be applied. Furthermore, the creep measurements may be complicated to be conducted reproducibly in the clinical environment.

In study III, significant site-dependent variations of the cartilage dynamic modulus and the ultrasound reflection coefficient were detected by using the ultrasound indentation instrument. The dynamic modulus was significantly higher in LPG as compared to MTP. The ultrasound reflection coefficient at the articular surface was significantly smaller at MTP, as compared to other test sites. Very similar site-dependent variation of dynamic modulus was revealed in study I (unconfined compression), as well as in previous studies [9, 99] which have investigated canine cartilage (indentation geometry). The ultrasound reflection coefficient was not related to the cartilage GAG content. Instead, it showed a similar site-dependent variation as the thickness of cartilage superficial zone [9, 99]. This suggests that there is a positive relationship between the ultrasound reflection and the thickness of the superficial zone in normal cartilage. To conclude, due to significant site-dependent variation of mechano-acoustic properties, cartilage parameters in the (normal) reference population should be classified according to the measurement site, in order to establish a reference database for the *in vivo* measurements.

Cartilage thickness is an essential clinical parameter and, if known, it enables a correct measurement of tissue modulus. It has been shown earlier that cartilage thickness can be measured by using ultrasound (and prefined sound speed) [114, 159]. In parallel to previous studies from our group [124, 161], only a minor or no decrease was found in the sound speed after PG or collagen degradation (II). With the ultrasound indentation instrument, the maximum detected change (-3.6%) in the

sound speed would have generated a +3.7% error in the estimation of the thickness and an error of ± 0.04% for dynamic modulus. In study IV, sound speed was further studied and its site-dependent variation was recorded. The results indicated that in the knee joint, the use of a predefined sound speed (1630 m/s = mean sound speed in the knee joint), would have induced a maximum error of 2.9 ± 3.8% (Patella) (mean ± 2SD) for the measurements of cartilage thickness. Similarly, in the knee joint, the maximum error incurred in dynamic modulus would have been 0.3 ± 0.6% (Patella). The sound speed in patellar cartilage was significantly related to the degenerative state of tissue, *i.e.* Mankin's score (range 0 - 10) although the minimum registered value (1555 m/s) was only 7.7% smaller than the maximum registered value (1685 m/s). According to recent findings of our group, sound speed in human knee joint cartilage is in the same range as in bovine cartilage (data not shown). This suggests that a constant sound speed can be utilized during ultrasound indentation measurements in order to obtain an acceptable accuracy for the measurements of cartilage thickness and dynamic modulus.

The ultrasound indentation method requires some experience on the part of the user. Recently, Appleyard et al. (2001) introduced a dynamic indentation probe [7], in which oscillation of the indenter was controlled electrically, *i.e.* cartilage deformation was not induced manually by the user. This is a technically favorable idea and a similar approach could further improve the ease of use of the ultrasound indentation instrument. This would be advantageous since the interoperator reliability for the dynamic modulus was only moderate (0.669). In clinical practice, the instrument may be used during ordinary arthroscopy and, therefore, the measurements can be carried out on those individuals who are suspected to be experiencing alterations in their cartilage. Another highly important area could be follow-up measurements, especially after cartilage repair surgery. In the future, it is believed that novel tissue engineering materials, which could simulate more realistically mature cartilage structure, will play an even a more salient role in the area of orthopaedics. Improved diagnostic methods could offer novel aspects also for clinical research. As a preclinical example, Appleyard et al. (2003) indicated with their dynamic indentation probe [7] that cartilage at tibial plateau softens significantly after knee meniscectomy in mature sheep [6].

In contrast to current diagnostic techniques, or to enhanced imaging techniques such as OCT, the technique presented herein provides direct quantitative information on cartilage functional properties. In study V, the reference material testing device was used for determining cartilage dynamic modulus in the visually normal and degenerated cartilage. The dynamic modulus was systematically low in the visually degenerated cartilage. More importantly, some of the visually intact samples also showed a low dynamic modulus, revealing that visually intact cartilage may already exhibit poor mechanical properties. Previously, it has been suggested that changes in cartilage functional properties may precede the structural changes in

the tissue matrix [5, 102]. The equilibrium Young's modulus correlated negatively with the cartilage Mankin's score. However, it was not as sensitive as the dynamic modulus in detecting the early degenerative changes.

Measurement of ultrasound reflection from the articular surface is a reliable (interoperator reliability = 0.786) and straightforward method for diagnosing the status of the superficial collagen network. It can be used for detecting visually undetectable signs of superficial degeneration. However, the external sleeve that was used in the prototype instrument cannot be used *in vivo*, and the design of the instrument must be modified for keeping the transducer at a known distance from the articular surface during ultrasound reflection measurements. In addition, due to the rather inhomogeneous structure of cartilage, the sensitivity of the stiffness measurements at detecting local tissue changes should be studied. In a recent study [144] the capability of the instrument to detect early spontaneous bovine cartilage degeneration was investigated. The early degenerative signs, indicated by a low Mankin's score (<2), were sensitively detected with the instrument as a decrease in both the dynamic modulus and the ultrasound reflection.

In addition to the A-mode ultrasound measurement, B-mode ultrasound imaging would provide additional, visual and possibly quantitative, information on the structure and composition of cartilage and subchondral bone. In study V, mechanical indentation measurements and ultrasound imaging were used for diagnosing porcine cartilage healing after ACT surgery. It was shown that the ultrasound imaging and mechanical indentation were complementary to each other and they provided valuable information on both the functional and structural integrity of cartilage and subchondral bone. The ultrasound imaging could also provide a means for the delineation of the repair area before the surgical intervention.

In study V, internal porcine cartilage was more echogenic compared with bovine cartilage. Based on our recent findings, the architecture of the collagen fibrils is subjected to significant remodeling during the maturation of the porcine [139], human, bovine and equine cartilage. In immature cartilage, the orientation of the collagen fibrils is highly tangential in all zones of the tissue and the cartilage may be vascular [139]. In study V, the pigs were less than 10 months old and immature. This suggests that the differences between the echogenity of porcine and bovine cartilage were, at least partially, related to the different maturation stage of the animals. Based on the encouraging findings of this thesis, further investigations towards more quantitative ultrasonic evaluation of cartilage and subchondral bone quality are in progress. However, in rough and curved surfaces, quantitative ultrasound reflection and backscattering parameters can be calculated reliably only from those sites which are perpendicular to the ultrasound beam [168].

In summary, the instrument developed in this study is capable of quantitative analysis of the mechanical properties of articular cartilage as well as of measuring tissue thickness. Furthermore, the ultrasound reflection can diagnose the status of

the superficial collagen network in a sensitive manner. Since the ultrasound indentation instrument possesses these combined qualities, it may provide significant advantages in the early clinical diagnosis of OA as well as in monitoring cartilage regeneration after surgical repair. However, prior to clinical use, the *in vivo* reproducibility of the ultrasound indentation measurements will have to be evaluated. In addition, further technical development and theoretical validation should take place before there can be any clinical application of the instrumentation.

CHAPTER X

Summary and conclusions

The following conclusions, based on the present experimental and numerical studies, can be drawn:

1. Collagen is the major determinant of cartilage dynamic stiffness, while the PGs primarily control the long-term mechanical properties, especially the equilibrium stiffness. This suggests that preferably both dynamic and time-dependent mechanical properties should be evaluated if one wishes to diagnose the quality of articular cartilage.

   The site-dependent variation of cartilage mechanical properties, as revealed in the present and some earlier studies, indicates that in order to diagnose cartilage properties *in vivo*, it is essential to compare the measured values with the site-matched reference values of the normal population.

2. A prototype of an arthroscopic ultrasound indentation instrument was developed and validated. This instrument permits the, combined measurement of tissue dynamic modulus, creep rate and ultrasound reflection from the cartilage surface and thus provides a sensitive method to distinguish between normal and degenerated cartilage. Ultrasound reflection is a sensitive and specific parameter for assessing superficial collagen disruption. When combined with the creep rate measurement, the ultrasound indentation method enables the differentiation of specific PG loss from collagen degradation.

3. Significant topographical variations of the cartilage dynamic modulus and the ultrasound reflection coefficient in the bovine knee joint were objectively detected with the ultrasound indentation technique.

4. The changes in composition of the cartilage (especially in the water content) may significantly affect the sound speed in articular cartilage. However, current findings suggest that a constant sound speed can be utilized during ultrasound indentation measurements, in order to obtain a clinically acceptable accuracy for evaluation of cartilage thickness and dynamic modulus.

5. Ultrasound imaging and mechanical indentation, as used for the evaluation of the success of ACT-surgery *in situ*, were complementary to each other in that they provided valuable information on both the structural and functional integrity of cartilage and subchondral bone. Mechanical measurements are superior to visual evaluation as indicators of cartilage quality. Furthermore, it was observed that qualitative ultrasound imaging may be used for the evaluation of cartilage degeneration.

Further technical and theoretical developments are needed before the ultrasound-indentation instrument can be used in clinical arthroscopy. These will include a novel method for keeping the transducer at a constant distance from the articular surface during the ultrasound reflection measurement, careful investigation of the reproducibility, as well as a more rigorous numerical modeling of the creep measurement.

REFERENCES

[1] Adam C, Eckstein F, Milz S, Schulte E, Becker C, and Putz R. The distribution of cartilage thickness in the knee-joints of old-aged individuals-measurement by A-mode ultrasound. *Clin Biomech*, 13:1–10, 1998.

[2] Adler RS, Dedrick DK, Laing TJ, Chiang EH, Meyer CR, Bland PH, and Rubin JM. Quantitative assessment of cartilage surface roughness in osteoarthritis using high frequency ultrasound. *Ultrasound Med Biol*, 18:51–58, 1992.

[3] Agemura DH, O'Brien (Jr) WD, Olerud JE, Chun LE, and Eyre DE. Ultrasonic propagation properties of articular cartilage at 100 MHz. *J Acoust Soc Am*, 87:1786–1791, 1990.

[4] Akizuki S, Mow VC, Muller F, Pita JC, Howell DS, and Manicourt DH. Tensile properties of human knee joint cartilage: I. Influence of ionic conditions, weight bearing, and fibrillation on the tensile modulus. *J Orthop Res*, 4:379–392, 1986.

[5] Altman RD, Tenenbaum J, Latta L, Riskin W, Blanco LN, and Howell DS. Biomechanical and biochemical properties of dog cartilage in experimentally induced osteoarthritis. *Ann Rheum Dis*, 43:83–90, 1984.

[6] Appleyard RC, Burkhardt D, Ghosh P, Read R, Cake M, Swain MV, and Murrell GAC. Topographical analysis of the structural, biochemical and dynamic biomechanical properties of cartilage in an ovine model of osteoarthritis. *Osteoarthritis Cartilage*, 11:65–77, 2003.

[7] Appleyard RC, Swain MV, Khanna S, and Murrell GAC. The accuracy and reliability of a novel handheld dynamic indentation probe for analysing articular cartilage. *Phys Med Biol*, 46:541–550, 2001.

[8] Armstrong CG and Mow VC. Variations in the intrinsic mechanical properties of human articular cartilage with age, degeneration, and water content. *J Bone Joint Surg Am*, 64:88–94, 1982.

[9] Arokoski JPA, Hyttinen MM, Helminen HJ, and Jurvelin JS. Biomechanical and structural characteristics of canine femoral and tibial cartilage. *J Biomed Mater Res*, 48:99–107, 1999.

[10] Arokoski JPA, Jurvelin JS, Väätäinen U, and Helminen HJ. Normal and patho-

logical adaptations of articular cartilage to joint loading. *Scand J Med Sci Sports*, 10:186–198, 2000.

[11] Ateshian GA. A theoretical formulation for boundary friction in articular cartilage. *J Biomech Eng*, 119:81–86, 1997.

[12] Ateshian GA and Soslowsky LJ. Human knee joint anatomy and cartilage thickness. *Transact Orthop Res Soc*, 17:619, 1992.

[13] Athanasiou KA, Constantinides G, and Lanctot DR. Articular cartilage evaluator and method for using the same. *United States Patent 5673708*, 1997.

[14] Athanasiou KA, Rosenwasser MP, Buckwalter JA, Malinin TI, and Mow VC. Interspecies comparisons of *in situ* intrinsic mechanical properties of distal femoral cartilage. *J Orthop Res*, 9:330–340, 1991.

[15] Bader DL and Kempson GE. The short-term compressive properties of adult human articular cartilage. *Biomed Mater Eng*, 4:245–256, 1994.

[16] Bader DL, Kempson GE, Egan J, Gilbey W, and Barrett AJ. The effects of selective matrix degradation on the short-term compressive properties of adult human articular cartilage. *Biochim Biophys Acta*, 1116:147–154, 1992.

[17] Bank RA, Bayliss MT, Lafeber FPJG, Maroudas A, and Tekoppele JM. Ageing and zonal variation in post-translational modification of collagen in normal human articular cartilage. The age-related increase in non-enzymatic glycation affects biomechanical properties of cartilage. *Biochem J*, 330:345–351, 1998.

[18] Bank RA, Soudry M, Maroudas A, Mizrahi J, and TeKoppele JM. The increased swelling and instantaneous deformation of osteoarthritic cartilage is highly correlated with collagen degradation. *Arthritis Rheum*, 43:2202–2210, 2000.

[19] Benninghoff A. Form und bau der gelenkknorpel in ihren beziehungen zur function. Erste mitteilung: Die modellierenden und formerhaltenden faktoren des knorpelreliefs. *Z Anat*, 76, 1925.

[20] Blake GM, Wahner HW, and Fogelman I. Assessment of instrument performance: Precision, installation of new equipment and radiation dose. In *The evaluation of osteoporosis: Dual energy X-ray absorptiometry and ultrasound in clinical practice*, pages 147–157. Martin Dunitz Ltd, London, 2nd edition, 1999.

[21] Blumenkrantz N and Asboe-Hansen G. New method for quantitative determination of uronic acids. *Anal Biochem*, 54:484–489, 1973.

[22] Brittberg M. Autologous chondrocyte transplantation. *Clin Orthop*, (367 Suppl):S147–155, 1999.

[23] Brittberg M, Lindahl A, Nilsson A, Ohlsson C, Isaksson O, and Peterson L. Treatment of deep cartilage defects in the knee with autologous chondrocyte transplantation. *N Engl J Med*, 331:889–895, 1994.

[24] Brown TD and Singerman RJ. Experimental determination of the linear biphasic constitutive coefficients of human fetal proximal femoral chondroepiphysis. *J Biomech*, 19:597–605, 1986.

[25] Buckwalter JA. Evaluating methods of restoring cartilaginous articular surfaces. *Clin Orthop*, (367 Suppl):S224–238, 1999.

[26] Buckwalter JA and Martin J. Degenerative joint disease. *Clin Symp*, 47:1–32, 1995.

[27] Buckwalter J and Mankin H. Articular cartilage, part II: Degeneration and osteoarthritis, repair, regeneration, and transplantation. *J Bone Joint Surg Am*, 79:612–632, 1997.

[28] Bursać PM, Obitz TW, Eisenberg SR, and Stamenović D. Confined and unconfined stress relaxation of cartilage: Appropriateness of a transversely isotropic analysis. *J Biomech*, 32:1125–1130, 1999.

[29] Burstein D, Bashir A, and Gray ML. MRI techniques in early stages of cartilage disease. *Invest Radiol*, 35:622–638, 2000.

[30] Buschmann MD, Soulhat J, Shirazi-Adl A, Jurvelin JS, and Hunziker EB. Confined compression of articular cartilage: Linearity in ramp and sinusoidal tests and the importance of interdigitation and incomplete confinement. *J Biomech*, 31:171–178, 1998.

[31] Campailla E, Causero A, Fogolari G, Mastidoro L, and Osti L. Prospects and advantages in the use of cartilage cell cultures for *in vivo* transplants. *Chir Organi Mov*, 84:355–358, 1999.

[32] Challis RE and Kitney RI. Biomedical signal processing. Part 1. Time-domain methods. *Med Biol Eng Comput*, 28:509–524, 1990.

[33] Chenevert TL, Bylski DI, Carson PL, Meyer CR, Bland PH, Adler DD, and Schmitt RM. Ultrasonic computed tomography of the breast. Improvement of image quality by use of cross-correlation time-of-flight and phase-insensitive attenuation measurements. *Radiology*, 152:155–159, 1984.

[34] Chiang EH, Adler RS, Meyer CR, Rubin JM, Dedrick DK, and Laing TJ. Quantitative assessment of surface roughness using backscattered ultrasound: The effects of finite surface curvature. *Ultrasound Med Biol*, 20:123–135, 1994.

[35] Chiang EH, Laing TJ, Meyer CR, Boes JL, Rubin JM, and Adler RS. Ultrasonic characterization of *in vitro* osteoarthritic articular cartilage with validation by confocal microscopy. *Ultrasound Med Biol*, 23:205–213, 1997.

[36] Chérin E, Saïed A, Laugier P, Netter P, and Berger G. Evaluation of acoustical parameter sensitivity to age-related and osteoarthritic changes in articular cartilage using 50 – MHz ultrasound. *Ultrasound Med Biol*, 24:341–354, 1998.

[37] Chérin E, Saïed A, Pellaumail B, Loeuille D, Laugier P, Gillet P, Netter P, and Berger G. Assessment of rat articular cartilage maturation using 50-MHz quantitative ultrasonography. *Osteoarthritis Cartilage*, 9:178–186, 2001.

[38] Clark JM. The organisation of collagen fibrils in the superficial zones of articular cartilage. *J Anat*, 171:117–130, 1990.

[39] Cohen B, Lai WM, and Mow VC. A transversely isotropic biphasic model for unconfined compression of growth plate and chondroepiphysis. *J Biomech Eng*, 120:491–496, 1998.

[40] Collins DH and McElliot TF. Sulphate ($^{35}SO_4$) uptake by chondrocytes in relation to histological changes in osteoarthritic human articular cartilage. *Ann rheum*, 19:318–330, 1960.

[41] Dashefsky JH. Arthroscopic measurement of chondromalacia of patella cartilage using a microminiature pressure transducer. *Arthroscopy*, 3:80–85, 1987.

[42] D'Astous FT and Foster FS. Frequency dependence of ultrasound attenuation and backscatter in breast tissue. *Ultrasound Med Biol*, 12:795–808, 1986.

[43] DiSilvestro MR and Suh JK. A cross-validation of the biphasic poroviscoelastic model of articular cartilage in unconfined compression, indentation, and confined compression. *J Biomech*, 34:519–525, 2001.

[44] DiSilvestro MR, Zhu Q, and Suh JK. Biphasic poroviscoelastic simulation of the unconfined compression of articular cartilage: II - Effect of variable strain rates. *J Biomech Eng*, 123:198–200, 2001.

[45] DiSilvestro MR, Zhu Q, Wong M, Jurvelin JS, and Suh JK. Biphasic poroviscoelastic simulation of the unconfined compression of articular cartilage: I – Simultaneous prediction of reaction force and lateral displacement. *J Biomech Eng*, 123:191–197, 2001.

[46] Disler DG, Raymond E, May DA, Wayne JS, and McCauley TR. Articular cartilage defects: *In vitro* evaluation of accuracy and interobserver reliability for detection and grading with US. *Radiology*, 215:846–851, 2000.

[47] Duck FA, Baker AC, and Starritt HC, editors. *Ultrasound in medicine*. Medical Science Series. Institute of Physics Publishing, London, 1998.

[48] Elders MJ. The increasing impact of arthritis on public health. *J Rheumatol Suppl*, 60:6–8, 2000.

[49] Elliott DM, Narmoneva DA, and Setton LA. Direct measurement of the Poisson's ratio of human patella cartilage in tension. *J Biomech Eng*, 124:223–228, 2002.

[50] Felson DT and Buckwalter J. Débridement and lavage for osteoarthritis of the knee. *N Engl J Med*, 347:132–133, 2002.

[51] Forster H and Fisher J. The influence of loading time and lubricant on the friction of articular cartilage. *Proc Inst Mech Eng [H]*, 210:109–119, 1996.

[52] Forster H and Fisher J. The influence of continuous sliding and subsequent surface wear on the friction of articular cartilage. *Proc Inst Mech Eng [H]*, 213:329–345, 1999.

[53] Fukui N, Purple CR, and Sandell LJ. Cell biology of osteoarthritis: The chondrocyte's response to injury. *Curr Rheumatol Rep*, 3:496–505, 2001.

[54] Gardner TR, Balaguer EJ, Ateshian GA, and Mow VC. Comparison of isotropic and transversely isotropic material properties from confined compression and indentation. *Transact ASME*, 50:715–716, 2001.

[55] Garon M, Guardo R, and Buschmann MD. Estimation and sensitivity to cartilage degradation of electromechanical coupling coefficents derived using spatially resolved streaming potentials. *Transact Orthop Res Soc*, 26:420, 2001.

[56] Geleskie JV and Shung KK. Further studies on acoustic impedance of major bovine blood vessel walls. *J Acoust Soc Am*, 71:467–470, 1982.

[57] Ghazavi MT, Pritzker KP, Davis AM, and Gross AE. Fresh osteochondral allografts for post-traumatic osteochondral defects of the knee. *J Bone Joint Surg Br*, 79:1008–1013, 1997.

[58] Gu WY, Lai WM, and Mow VC. Transport of fluid and ions through a porous-permeable charged-hydrate tissue, and streaming potential data on normal bovine

articular cartilage. *J Biomech*, 26:709–723, 1993.

[59] Gu WY, Lai WM, and Mow VC. A triphasic analysis of negative osmotic flows through charged hydrated soft tissues. *J Biomech*, 30:71–78, 1997.

[60] Gu WY, Lai WM, and Mow VC. A mixture theory for charged-hydrated soft tissues containing multi- electrolytes: Passive transport and swelling behaviors. *J Biomech Eng*, 120:169–180, 1998.

[61] Guilak F, Butler DL, and Goldstein SA. Functional tissue engineering: The role of biomechanics in articular cartilage repair. *Clin Orthop*, (391 Suppl):S295–305, 2001.

[62] Guilak F, Ratcliffe A, and Mow VC. Chondrocyte deformation and local tissue strain in articular cartilage: A confocal microscopy study. *J Orthop Res*, 13:410–421, 1995.

[63] Haapala J, Arokoski JPA, Hyttinen MM, Lammi M, Tammi M, Kovanen V, Helminen HJ, and Kiviranta I. Remobilization does not fully restore immobilization induced articular cartilage atrophy. *Clin Orthop*, (362):218–229, 1999.

[64] Hangody L, Kish G, Kárpáti Z, Szerb I, and Udvarhelyi I. Arthroscopic autogenous osteochondral mosaicplasty for the treatment of femoral condylar articular defects. A preliminary report. *Knee Surg Sports Traumatol Arthrosc*, 5:262–267, 1997.

[65] Hangody L, Kish G, Kárpáti Z, Udvarhelyi I, Szigeti I, and Bely M. Mosaicplasty for the treatment of articular cartilage defects: Application in clinical practice. *Orthopedics*, 21:751–756, 1998.

[66] Harris (Jr) ED, Parker HG, Radin EL, and Krane SM. Effects of proteolytic enzymes on structural and mechanical properties of cartilage. *Arthritis Rheum*, 15:497–503, 1972.

[67] Hasler EM, Herzog W, Wu JZ, Müller W, and Wyss U. Articular cartilage biomechanics: Theoretical models, material properties, and biosynthetic response. *Crit Rev Biomed Eng*, 27:415–488, 1999.

[68] Hayes WC and Bodine AJ. Flow-independent viscoelastic properties of articular cartilage matrix. *J Biomech*, 11:407–419, 1978.

[69] Hayes WC, Keer LM, Herrmann G, and Mockros LF. A mathematical analysis for indentation tests of articular cartilage. *J Biomech*, 5:541–551, 1972.

[70] Hayes (Jr) DW, Brower RL, and John KJ. Articular cartilage. Anatomy, injury, and repair. *Clin Podiatr Med Surg*, 18:35–53, 2001.

[71] Hedlund H, Mengarelli-Widholm S, Reinholt FP, and Svensson O. Stereologic studies on collagen in bovine articular cartilage. *Apmis*, 101:133–140, 1993.

[72] Herrmann JM, Pitris C, Bouma BE, Boppart SA, Jesser CA, Stamper DL, Fujimoto JG, and Brezinski ME. High resolution imaging of normal and osteoarthritic cartilage with optical coherence tomography. *J Rheumatol*, 26:627–635, 1999.

[73] Hirvonen J, Laasanen MS, Töyräs J, Saarakkala S, and Jurvelin JS. Novel ultrasound indentation instrument and software for mechano-acoustic evaluation of articular cartilage. *Acta Bioeng Biomech*, 4:447–448, 2002.

[74] Huang CY, Mow VC, and Ateshian GA. The role of flow-independent viscoelasticity in the biphasic tensile and compressive responses of articular cartilage. *J Biomech*

Eng, 123:410–417, 2001.

[75] Huang D, Swanson EA, Lin CP, Schuman JS, Stinson WG, Chang W, Hee MR, Flotte T, Gregory K, Puliafito CA, and Fujimoto JG. Optical coherence tomography. *Science*, 254:1178–1181, 1991.

[76] Hunter W. Of the structure and disease of articulating cartilages. *Philos Trans R Soc Lond*, 42:514–521, 1743.

[77] Hunziker EB. Articular cartilage repair: Basic science and clinical progress. A review of the current status and prospects. *Osteoarthritis Cartilage*, 10:432–463, 2002.

[78] Joiner GA, Bogoch ER, Pritzker KP, Buschmann MD, Chevrier A, and Foster FS. High frequency acoustic parameters of human and bovine articular cartilage following experimentally-induced matrix degradation. *Ultrason Imaging*, 23:106–116, 2001.

[79] Jones IL, Larsson SE, and Lemperg R. The glycosaminoglycans of human articular cartilage: Concentration and distribution in different layers in the adult individual. *Clin Orthop*, 127:257–264, 1977.

[80] Joseph D, Gu WY, Mao XG, Lai WM, and Mow VC. True density of normal and enzymatically treated bovine articular cartilage. *Transact Orthop Res Soc*, 24:642, 1999.

[81] Jurvelin JS, Arokoski JPA, Hunziker EB, and Helminen HJ. Topographical variation of the elastic properties of articular cartilage in the canine knee. *J Biomech*, 33:669–675, 2000.

[82] Jurvelin JS, Buschmann MD, and Hunziker EB. Optical and mechanical determination of Poisson's ratio of adult bovine humeral articular cartilage. *J Biomech*, 30:235–241, 1997.

[83] Jurvelin JS, Buschmann MD, and Hunziker EB. Mechanical anisotropy of the human knee articular cartilage in compression. *Proc Inst Mech Eng [H]*, 217:215–219, 2003.

[84] Kalunian KC, Moreland LW, Klashman DJ, Brion PH, Concoff AL, Myers S, Singh R, Ike RW, Seeger LL, Rich E, and Skovron ML. Visually-guided irrigation in patients with early knee osteoarthritis: A multicenter randomized, controlled trial. *Osteoarthritis Cartilage*, 8:412–418, 2000.

[85] Kawchuk GN and Elliott PD. Validation of displacement measurements obtained from ultrasonic images during indentation testing. *Ultrasound Med Biol*, 24:105–111, 1998.

[86] Kempson GE. Relationship between the tensile properties of articular cartilage from the human knee and age. *Ann Rheum Dis*, 41:508–511, 1982.

[87] Kempson GE. Age-related changes in the tensile properties of human articular cartilage: A comparative study between the femoral head of the hip joint and the talus of the ankle joint. *Biochim Biophys Acta*, 1075:223–230, 1991.

[88] Kempson GE, Freeman MA, and Swanson SA. Tensile properties of articular cartilage. *Nature*, 220:1127–1128, 1968.

[89] Kempson GE, Muir H, Pollard C, and Tuke M. The tensile properties of the cartilage of human femoral condyles related to the content of collagen and glycosaminogly-

cans. *Biochim Biophys Acta*, 297:456–472, 1973.

[90] Kempson GE, Spivey CJ, Swanson SAV, and Freeman MAR. Patterns of cartilage stiffness on normal and degenerate human femoral heads. *J Biomech*, 4:597–609, 1971.

[91] Kempson GE, Tuke MA, Dingle JT, Barrett AJ, and Horsfield PH. The effects of proteolytic enzymes on the mechanical properties of adult human articular cartilage. *Biochim Biophys Acta*, 428:741–760, 1976.

[92] Kiefer GN, Sundby K, McAllister D, Shrive NG, Frank CB, Lam T, and Schachar NS. The effect of cryopreservation on the biomechanical behavior of bovine articular cartilage. *J Orthop Res*, 7:494–501, 1989.

[93] Kim HK, Babyn PS, Harasiewicz KA, Gahunia HK, Pritzker KPH, and Foster FS. Imaging of immature articular cartilage using ultrasound backscatter microscopy at 50 MHz. *J Orthop Res*, 13:963–970, 1995.

[94] Király K, Lammi M, Arokoski J, Lapveteläinen T, Tammi M, Helminen H, and Kiviranta I. Safranin O reduces loss of glycosaminoglycans from bovine articular cartilage during histological specimen preparation. *Histochem J*, 28:99–107, 1996.

[95] Korhonen RK, Laasanen MS, Töyräs J, Helminen HJ, and Jurvelin JS. Superficial collagen network modifies differently equilibrium response of articular cartilage in unconfined compression and indentation. *Transact Orthop Res Soc*, 27:79, 2002.

[96] Korhonen RK, Laasanen MS, Töyräs J, Lappalainen R, Helminen HJ, and Jurvelin JS. Fibril reinforced poroelastic model predicts specifically mechanical behaviour of normal, proteoglycan depleted and collagen degraded articular cartilage. *J Biomech*, 36:1373–1379, 2003.

[97] Korhonen RK, Laasanen MS, Töyräs J, Rieppo J, Hirvonen J, Helminen HJ, and Jurvelin JS. Comparison of the equilibrium response of articular cartilage in unconfined compression, confined compression and indentation. *J Biomech*, 35:903–909, 2002.

[98] Korhonen RK, Töyräs J, Nieminen MT, Rieppo J, Hirvonen J, Helminen HJ, and Jurvelin JS. Effect of ionic environment on the compression-tension nonlinearity of articular cartilage in the direction perpenticular to articular surface. *Transact Orthop Res Soc*, 26:439, 2001.

[99] Korhonen RK, Wong M, Arokoski J, Lindgren R, Helminen HJ, Hunziker EB, and Jurvelin JS. Importance of the superficial tissue layer for the indentation stiffness of articular cartilage. *Med Eng Phys*, 24:99–108, 2002.

[100] Krishnan R, Kopacz M, and Ateshian GA. Verification of the role of interstitial fluid load support in the frictional response of bovine articular cartilage. *Transact Orthop Res Soc*, 28:287, 2003.

[101] Lai WM, Hou JS, and Mow VC. A triphasic theory for the swelling and deformation behaviors of articular cartilage. *J Biomech Eng*, 113:245–258, 1991.

[102] Lane JM, Chisena E, and Black J. Experimental knee instability: Early mechanical property changes in articular cartilage in a rabbit model. *Clin Orthop*, (140):262–265, 1979.

[103] Lee RC, Frank EH, Grodzinsky AJ, and Roylance DK. Oscillatory compressional

behavior of articular cartilage and its associated electromechanical properties. *J Biomech Eng*, 103:280–292, 1981.

[104] Lefebvre F, Graillat N, Chérin E, Berger G, and Saïed A. Automatic three-dimensional reconstruction and characterization of articular cartilage from high-resolution ultrasound acquisitions. *Ultrasound Med Biol*, 24:1369–1381, 1998.

[105] Légaré A, Garon M, Guardo R, Savard P, Poole AR, and Buschmann MD. Detection and analysis of cartilage degeneration by spatially resolved streaming potentials. *J Orthop Res*, 20:819–826, 2002.

[106] Li LP, Soulhat J, Buschmann MD, and Shirazi-Adl A. Nonlinear analysis of cartilage in unconfined ramp compression using a fibril reinforced poroelastic model. *Clin Biomech*, 14:673–682, 1999.

[107] Lyyra T. *Development, validation and clinical application of indentation technique for arthroscopic measurement of cartilage stiffness.* PhD thesis, University of Kuopio, 1997.

[108] Lyyra T, Jurvelin J, Pitkänen P, Väätäinen U, and Kiviranta I. Indentation instrument for the measurement of cartilage stiffness under arthroscopic control. *Med Eng Phys*, 17:395–399, 1995.

[109] Lyyra T, Kiviranta I, Väätäinen U, Helminen HJ, and Jurvelin JS. *In vivo* characterization of indentation stiffness of articular cartilage in the normal human knee. *J Biomed Mater Res*, 48:482–487, 1999.

[110] Mak AF. The apparent viscoelastic behavior of articular cartilage –The contributions from the intrinsic matrix viscoelasticity and interstitial fluid flows. *J Biomech Eng*, 108:123–130, 1986.

[111] Mak AF, Lai WM, and Mow VC. Biphasic indentation of articular cartilage. I. Theoretical analysis. *J Biomech*, 20:703–714, 1987.

[112] Mankin HJ, Dorfman H, Lippiello L, and Zarins A. Biochemical and metabolic abnormalities in articular cartilage from osteo-arthritic human hips. II. Correlation of morphology with biochemical and metabolic data. *J Bone Joint Surg Am*, 53:523–537, 1971.

[113] Mann RW. Comment on 'Ultrasonic measurement of the thickness of human articular cartilage *in situ*' by Yao and Seedhom. *Rheumatology*, 40:829–831, 2001.

[114] Modest VE, Murphy MC, and Mann RW. Optical verification of a technique for *in situ* ultrasonic measurement of articular cartilage thickness. *J Biomech*, 22:171–176, 1989.

[115] Moseley JB, O'Malley K, Petersen NJ, Menke TJ, Brody BA, Kuykendall DH, Hollingsworth JC, Ashton CM, and Wray NP. A controlled trial of arthroscopic surgery for osteoarthritis of the knee. *N Engl J Med*, 347:81–88, 2002.

[116] Mow VC, Fithian DC, and Kelly MA. Fundamentals of articular cartilage and meniscus biomechanics. In Ewing JW, editor, *Articular cartilage and knee joint function: Basic science and arthroscopy*, pages 1–18. Raven Press Ltd, New York, 1990.

[117] Mow VC and Guo XE. Mechano-electrochemical properties of articular cartilage: Their inhomogeneities and anisotropies. *Annu Rev Biomed Eng*, 4:175–209, 2002.

[118] Mow VC and Hayes WC. *Basic orthopaedic biomechanics.* Raven Press, New York, 1991.

[119] Mow VC, Kuei SC, Lai WM, and Armstrong CG. Biphasic creep and stress relaxation of articular cartilage in compression: Theory and experiments. *J Biomech Eng*, 102:73–84, 1980.

[120] Mow VC and Wang CC. Some bioengineering considerations for tissue engineering of articular cartilage. *Clin Orthop*, (367 Suppl):S204–223, 1999.

[121] Myers SL, Dines K, Brandt DA, Brandt KD, and Albrecht ME. Experimental assessment by high frequency ultrasound of articular cartilage thickness and osteoarthritic changes. *J Rheumatol*, 22:109–116, 1995.

[122] Nicholson PHF, Lowet G, Langton CM, Dequeker J, and Van der Perre G. A comparison of time-domain and frequency-domain approaches to ultrasonic velocity measurement in trabecular bone. *Phys Med Biol*, 41:2421–2435, 1996.

[123] Niederauer MQ, Cristante S, Niederauer GM, Wilkes RP, Singh SM, Messina DF, Walter MA, Boyan BD, DeLee JC, and Niederauer G. A novel instrument for quantitatively measuring the stiffness of articular cartilage. *Transact Orthop Res Soc*, 23:905, 1998.

[124] Nieminen HJ, Töyräs J, Rieppo J, Nieminen MT, Hirvonen J, Korhonen R, and Jurvelin JS. Real-time ultrasound analysis of articular cartilage degradation *in vitro*. *Ultrasound Med Biol*, 28:519 525, 2002.

[125] Nieminen MT, Rieppo J, Töyräs J, Hakumäki JM, Silvennoinen MJ, Hyttinen MM, Helminen HJ, and Jurvelin JS. T_2 relaxation reveals spatial collagen architecture in articular cartilage: A comparative quantitative MRI and polarized light microscopic study. *Magn Reson Med*, 46:487–493, 2001.

[126] Nieminen MT, Töyräs J, Laasanen MS, Silvennoinen J, Helminen HJ, and Jurvelin JS. Prediction of biomechanical properties of articular cartilage with quantitative magnetic resonance imaging. In press. *J Biomech*, 2003.

[127] Nieminen MT, Töyräs J, Rieppo J, Hakumäki JM, Silvennoinen J, Helminen HJ, and Jurvelin JS. Quantitative MR microscopy of enzymatically degraded articular cartilage. *Magn Reson Med*, 43:676–681, 2000.

[128] Njeh CF, Hans D, Fuerst T, Glüer CC, and Genant HK. *Quantitative ultrasound: Assessment of osteoporosis and bone status.* Martin Dunitz Ltd, London, 1999.

[129] Njeh CF, Hans D, Li J, Fan B, Fuerst T, He YQ, Tsuda-Futami E, Lu Y, Wu CY, and Genant HK. Comparison of six calcaneal quantitative ultrasound devices: Precision and hip fracture discrimination. *Osteoporos Int*, 11:1051–1062, 2000.

[130] Njeh CF and Langton CM. The effect of cortical endplates on ultrasound velocity through the calcaneus: An *in vitro* study. *Br J Radiol*, 70:504–510, 1997.

[131] Palmoski MJ and Brandt KD. Running inhibits the reversal of atrophic changes in canine knee cartilage after removal of a leg cast. *Arthritis Rheum*, 24:1329–1337, 1981.

[132] Panula HE, Hyttinen MM, Arokoski JPA, Långsjö TK, Pelttari A, Kiviranta I, and Helminen HJ. Articular cartilage superficial zone collagen birefringence reduced and cartilage thickness increased before surface fibrillation in experimental osteoarthri-

tis. *Ann Rheum Dis*, 57:237–245, 1998.

[133] Parsons JR and Black J. The viscoelastic shear behavior of normal rabbit articular cartilage. *J Biomech*, 10:21–29, 1977.

[134] Pellaumail B, Watrin A, Loeuille D, Netter P, Berger G, Laugier P, and Saïed A. Effect of articular cartilage proteoglycan depletion on high frequency ultrasound backscatter. *Osteoarthritis Cartilage*, 10:535–541, 2002.

[135] Quenneville E, Garon M, Légaré A, and Buschmann MD. Load and streaming potential responses of articular cartilage as a function of compression speed during indentation. *Transact Orthop Res Soc*, 28:659, 2003.

[136] Ragozzino M. Analysis of the error in measurement of ultrasound speed in tissue due to waveform deformation by frequency-dependent attenuation. *Ultrasonics*, 19:135–138, 1981.

[137] Redler I. A scanning electron microscopic study of human normal and osteoarthritic articular cartilage. *Clin Orthop*, (103):262–268, 1974.

[138] Rieppo J, Hallikainen J, Jurvelin JS, Helminen HJ, and Hyttinen MM. Novel quantitative polarization microscopic assessment of cartilage and bone collagen birefringence, orientation and anisotropy. *Transact Orthop Res Soc*, 28:570, 2003.

[139] Rieppo J, Hyttinen MM, Halmesmäki E, Ruotsalainen H, Vasara A, Kiviranta I, Jurvelin JS, and Helminen HJ. Remodelation of collagen network architecture during cartilage maturation. In press. *Osteoarthritis Cartilage*, 2003.

[140] Rieppo J, Siitonen U, Halmesmäki EP, Laasanen MS, Töyräs J, Saarakkala S, Kiviranta I, Hyttinen MM, Jurvelin JS, and Helminen HJ. FTIR-characterization of human patellar cartilage - comparison to light microscopy and mechanical testing. *Transact Orthop Res Soc*, 28:290, 2003.

[141] Rieppo J, Töyräs J, Nieminen MT, Kovanen V, Hyttinen MM, Korhonen RK, Jurvelin JS, and Helminen HJ. Structural-function relationships in articular cartilage modified by enzymatic treatments. In press. *Cells Tissues Organs*, 2003.

[142] Roth V and Mow VC. The intrinsic tensile behavior of the matrix of bovine articular cartilage and its variation with age. *J Bone Joint Surg Am*, 62:1102–1117, 1980.

[143] Rushfeldt PD, Mann RW, and Harris WH. Improved techniques for measuring *in vitro* the geometry and pressure distribution in the human acetabulum–I. Ultrasonic measurement of acetabular surfaces, sphericity and cartilage thickness. *J Biomech*, 14:253–260, 1981.

[144] Saarakkala S, Laasanen MS, Jurvelin JS, Törrönen K, Lammi MJ, Lappalainen R, and Töyräs J. Ultrasound indentation of normal and spontaneously degenerated bovine articular cartilage. *Osteoarthritis Cartilage*, 11:697–705, 2003.

[145] Sachs JR and Grodzinsky AJ. Electromechanical spectroscopy of cartilage using a surface probe with applied mechanical displacement. *J Biomech*, 28:963–976, 1995.

[146] Saïed A, Chérin E, Gaucher H, Laugier P, Gillet P, Floquet J, Netter P, and Berger G. Assessment of articular cartilage and subchondral bone: Subtle and progressive changes in experimental osteoarthritis using 50MHz echography *in vitro*. *J Bone Miner Res*, 12:1378–1386, 1997.

[147] Santavirta S. Arthroscopy for osteoarthrosis of the knee is seldom necessary. *Acta*

Orthop Scand, 74:4–5, 2003.

[148] Schinagl RM, Gurskis D, Chen AC, and Sah RL. Depth-dependent confined compression modulus of full-thickness bovine articular cartilage. *J Orthop Res*, 15:499–506, 1997.

[149] Schwartz DE, Choi Y, Sandell LJ, and Hanson WR. Quantitative analysis of collagen, protein and DNA in fixed, paraffin-embedded and sectioned tissue. *Histochem J*, 17:655–663, 1985.

[150] Senzig DA, Forster FK, and Olerud JE. Ultrasonic attenuation in articular cartilage. *J Acoust Soc Am*, 92:676–681, 1992.

[151] Shingleton WD, Hodges DJ, Brick P, and Cawston TE. Collagenase: A key enzyme in collagen turnover. *Biochem Cell Biol*, 74:759–775, 1996.

[152] Siegel S and Castellan (Jr) NJ. The case of k independent samples. In Anker JD, editor, *Nonparametric statistics for the behaviour sciences*, pages 206–215. McGraw-Hill book company, Singapore, 2nd edition, 1988.

[153] Simon WH. Scale effects in animal joints. I. Articular cartilage thickness and compressive stress. *Arthritis Rheum*, 13:244–256, 1970.

[154] Soltz MA and Ateshian GA. A conewise linear elasticity mixture model for the analysis of tension-compression nonlinearity in articular cartilage. *J Biomech Eng*, 122:576–586, 2000.

[155] Soulhat J, Buschmann MD, and Shirazi-Adl A. A fibril-network-reinforced biphasic model of cartilage in unconfined compression. *J Biomech Eng*, 121:340–347, 1999.

[156] Stockwell RA and Meachim G. The chondrocytes. In Freeman MAR, editor, *Adult articular cartilage*, pages 51–99. Pitman medical, London, 1973.

[157] Strelitzki R, Clarke AJ, and Evans JA. The measurement of the velocity of ultrasound in fixed trabecular bone using broadband pulses and single-frequency tone bursts. *Phys Med Biol*, 41:743–753, 1996.

[158] Suh JK and Spilker RL. Indentation analysis of biphasic articular cartilage: Nonlinear phenomena under finite deformation. *J Biomech Eng*, 116:1–9, 1994.

[159] Suh JK, Youn I, and Fu FH. An *in situ* calibration of an ultrasound transducer: A potential application for an ultrasonic indentation test of articular cartilage. *J Biomech*, 34:1347–1353, 2001.

[160] Sun Y, Luo Z, and An K. Mechanical properties of single type II collagen molecule. *Transact Orthop Res Soc*, 27:82, 2002.

[161] Töyräs J, Rieppo J, Nieminen MT, Helminen HJ, and Jurvelin JS. Characterization of enzymatically induced degradation of articular cartilage using high frequency ultrasound. *Phys Med Biol*, 44:2723–2733, 1999.

[162] Tyyni A and Karlsson J. Biological treatment of joint cartilage damage. *Scand J Med Sci Sports*, 10:249–265, 2000.

[163] Vasara A, Nieminen MT, Peterson L, Jurvelin JS, and Kiviranta I. *In vivo* assessment of autologous chondrocyte transplantation using arthroscopic stiffness measurement and quantitative MRI of proteoglycans. *Transact Orthop Res Soc*, 27:458, 2002.

[164] Wang CCB, Chahine NO, Hung CT, and Ateshian GA. Optical determination

of anisotropic material properties of bovine articular cartilage in compression. *J Biomech*, 36:339–353, 2003.

[165] Wang CCB, Deng JM, Ateshian GA, and Hung CT. An automated approach for direct measurement of two-dimensional strain distributions within articular cartilage under unconfined compression. *J Biomech Eng*, 124:557–567, 2002.

[166] Wells PNT. *Physical Principles of Ultrasonic Diagnosis*. Academic Press, London, 1969.

[167] Wells PNT. *Biomedical Ultrasonics*. Academic Press, London, 1977.

[168] Wilhjelm JE, Pedersen PC, and Jacobsen SM. The influence of roughness, angle, range, and transducer type on the echo signal from planar interfaces. *IEEE Trans Ultrason Ferroelectr Freq Control*, 48:511–521, 2001.

[169] Wilson W, van Rietbergen B, van Donkelaar CC, and Huiskes R. Pathways of load-induced cartilage damage causing cartilage degeneration in the knee after meniscectomy. *J Biomech*, 36:845–851, 2003.

[170] Wong M, Ponticiello M, Kovanen V, and Jurvelin JS. Volumetric changes of articular cartilage during stress relaxation in unconfined compression. *J Biomech*, 33:1049–1054, 2000.

[171] Xia Y, Moody JB, Burton-Wurster N, and Lust G. Quantitative *in situ* correlation between microscopic MRI and polarized light microscopy studies of articular cartilage. *Osteoarthritis Cartilage*, 9:393–406, 2001.

[172] Yamagata T, Saito H, Habuchi O, and Suzuki S. Purification and properties of bacterial chondroitinases and chondrosulfatases. *J Biol Chem*, 243:1523–1535, 1968.

[173] Yao JQ and Seedhom BB. Ultrasonic measurement of the thickness of human articular cartilage *in situ*. *Rheumatology*, 38:1269–1271, 1999.

[174] Yelin E and Callahan LF. The economic cost and social and psychological impact of musculoskeletal conditions. National arthritis data work groups. *Arthritis Rheum*, 38:1351–1362, 1995.

[175] Zhang M, Zheng YP, and Mak AFT. Estimating the effective Young's modulus of soft tissues from indentation tests - Nonlinear finite element analysis of effects of friction and large deformation. *Med Eng Phys*, 19:512–517, 1997.

[176] Zheng YP, Ding CX, Bai J, Mak AFT, and Qin L. Measurement of the layered compressive properties of trypsin-treated articular cartilage: An ultrasound investigation. *Med Biol Eng Comput*, 39:534–541, 2001.

[177] Zheng YP and Mak AF. An ultrasound indentation system for biomechanical properties assessment of soft tissues *in-vivo*. *IEEE Trans Biomed Eng*, 43:912 918, 1996.